ULTRAFILTRATION OF SYNTHETIC PALM OIL MILL EFFLUENT (POME) USING PVDF AND α-AL_2O_3 MEMBRANES

by

Jiamin Wu

November 2020

in partial fulfillment of the requirements for the degree of

Master of Science
in Environmental Engineering

Supervisors: Prof.dr.ir Jules van Lier
Assis.Prof.dr.ir Ralph Lindeboom
Assoc.Prof.dr.ir Bas Heijman
Ir. Saqr AI-Muraisy

Jiamin Wu: *Ultrafiltration of Synthetic Palm Oil Mill Effluent (POME) using PVDF and α-Al_2O_3 Membranes* (2020)

Location: Water Lab
Department of Sanitary Engineering
Faculty of Civil Engineering and Geoscience & Environmental Engineering
Delft University of Technology

Supervisors: Prof.dr.ir Jules van Lier
Assis.Prof.dr.ir Ralph Lindeboom
Assoc.Prof.dr.ir Bas Heijman
Ir. Saqr AI-Muraisy

Defense: 13, November, 2020

ABSTRACT

In palm oil extraction process, a large amount of lipids are emulsified in waste stream and the hot, brownish palm oil mill effluent (POME) is generated. In this study, the membrane technology was proposed to test the feasibility of direct ultrafiltration (UF) of POME by using α-Al_2O_3 and PVDF membranes, and to figure out the recovery rates of water and oi. POME synthesis methodology was successfully generated in the lab with the oil droplet size distribution and oil concentration conforming to the characteristics of real POME. The optimal operating conditions for POME filtration was determined by executing ultrafiltration experiments at different permeate fluxes and pHs. Both membrane shown good performance at original POME pH (pH 5). Compared with PVDF membrane, Al_2O_3 shown great strengths in higher optimal flux (57LMH), lower required trans-membrane pressure (TMP), higher oil and water recovery. The formation of oil layer on Al_2O_3 membrane reversed the charge type of membrane surface, which transformed oil droplet-membrane attraction to oil droplet-oil layer repulsion that allowed for the higher rejection and steady filtration process. The effect of SDS surfactant was also studied to clarify whether it could significantly improve membrane performance. The addition of SDS brought in extra pollutant with the SDS micelle size smaller than membrane pores, which reduced permeate quality and increased fouling in UF process. In the aspect of process stability, SDS benefited α-Al_2O_3 membrane performance more than PVDF membrane. The bi-layers SDS formed on α-Al_2O_3 membrane resulted in charge inversion and increased hydrophilicity of membrane surface that respectively enhanced anti-fouling property and membrane permeability. In the long run, SDS addition stabilized TMP variation process and prevented the sharp TMP increase. However, to guarantee the permeate quality of membrane technology, SDS was not recommended to be added. To operate POME process with more stable TMP and less fouling, α-Al_2O_3 membrane was highly recommended for POME treatment with great potential of industrial application in the future.

The discussion of pH effect on membrane performance reveals other important affecting factors other than pH. Severe fouling of PVDF membrane happened below IEP_{PVDF} (pH 2). The increased hydrophobicity caused by oil layer formation could explain the lower membrane permeability and the adsorption of more hydrolyzed LCFA in acidic condition led to larger proportion of irreversible fouling. While the less excellent α-Al_2O_3 membrane performance at pH 10 was mainly due to the adsorption of more LCFA and glycerol onto membrane, despite the membrane-molecules/oil droplets repulsion existed in ultrafiltration. Although the general filtration mechanisms involves in almost all cases, the most important interactions that mainly function vary with different membrane and feed type.

ACKNOWLEDGEMENT

Thanks to the people involved in my master thesis project, I always felt motivated to face the challenges and solve the problems with confidence. Here I would like to thank them who offered help and contributed to this project.

Firstly, I would like to thank my daily supervisor, Saqr, who provided continuous support, and always encouraged me to communicate and share my opinions. I benefited a lot from the interactions with committee members and my labmates throughout my thesis project. I am also grateful to have Ralph as my supervisor, who was always patient to help me with the problems and paid much attention to the details. The advice given by him really helped me to get new findings from different perspectives and analyze results in depth. I would like to also thank Bas and Mingliang. They provided experimental setup, corrected my errors on time and helped me with the explanation of experimental results. I also appreciate Jules' comments on my thesis scope and the focus of this project.

I would also like to thank my parents for their unconditional support and caring, especially in the COVID-19 period. They gave me the chance to study abroad and pursue my dreams. In TU Delft, I am grateful to meet Ziwei, Mingyue and all my Chinese classmates of Environmental Engineering track. They were always willing to help me with any small staff thing with patience and their company made me feel happy in the lab. I would also like to thank Jianyi who always encouraged and took care of me. Her trust made me become more confident about my work.

CONTENTS

LIST OF FIGURES

LIST OF TABLES

ACRONYMS

1 INTRODUCTION

In current industry filed, oily wastewater is a significant concern, generated from various industries such as food, petrochemical, metallurgical, pharmaceutical, and oil gas, widely occurring in extraction, refining, transportation and storage processes of these industries [Yu et al., 2017; Ahmad and Ghufran, 2019]. Normally, oil presents in wastewater in three forms with different droplet sizes, free oil($(\geq 150\mu m$), emulsified oil ($<20\mu m$) and dissolved oil containing water soluble components [Ahmad et al., 2020]. Despite the threat on water body, soil and air quality posed by oily contaminants, the wastewater with small oil droplets ($<20\mu m$) is rather puzzling because many traditional physio-chemical methods are facing many challenges [Padaki et al., 2015; Ahmad et al., 2020]. To efficiently treat oily wastewater and reduce its environmental impacts, the membrane technology was comprehensively researched and subsequently applied in real industries for produced water treatment, with the strengths of high rejection rate and simple operation [Ahmad et al., 2020].

Palm oil mill effluent (POME) is a typical agricultural oily wastewater produced in the production process of Crude palm oil (CPO). In addition to the small size of emulsified oil that is hard to be treated, the huge quantity and high oil concentration (typically 4g/L) made POME as a concern in local places [Rupani et al., 2010; Ahmad and Ghufran, 2019]. Taking Malaysia as a representative palm oil producer, 32.25% global market share of palm oil brings about the generation of a huge quantity of POME (e.g. 178.9 million tons POME produced in 2017)[Oilseeds, 2019; Norhidayu et al., 2017; Ahmad and Ghufran, 2019]. The discharge of POME that is not well treated causes many environmental issues. Apart from the physical states (color and turbidity) that may significantly affect human sense, the high BOD of oily wastewater leads to oxygen depletion in the nearby water body thus many water based lives are not able to survive anymore. When making the choice of wastewater treatment methodology, the oil and other organic matter like long chain fatty acid (LCFA) are expected to be recovered to produce technical grade oil (TGO) or to be sent back to the palm oil production line. Thus the efficient methodology, membrane filtration was proposed to treat POME with the potentials of oil recovery from concentrate side.

In this study, both polymeric (Polyvinylidene fluoride (PVDF)) and ceramic membrane (Al_2O_3) will be tested at different parameter settings to determine their optimal operational conditions, discuss the feasibility of membrane filtration methodology for treating high-lipid wastewater, and to compare filtration performance and application potential of both membranes. As ceramic membrane can tolerate wider range of temperature with higher upper limit than PVDF membrane, ceramic membrane is expected to work at 90°C in filtration practice and other methods like hyper/thermophilic anaerobic membrane bioreactor. Thus this study can be a preliminary test before high-temperature research and application.

Besides, the surfactant will also be added in POME to clarify its function in oil separation. In many industrial processes, oily wastewater is produced originally with surfactants in it as one of the pollutants. However, in the palm oil extraction line, POME is generated without any addition of chemicals, thus whether the ex-

pected effect of surfactant manually added in POME on membrane performance modification can compensate the potential problems it brings about, needs to be discussed comprehensively. Besides, despite the general mechanisms of membrane filtration like electrostatic interaction and pore sieving, this study also discussed the effect of surfactant addition on the variation of membrane filtration mechanism.

2 LITERATURE

2.1 PALM OIL MILL EFFLUENT (POME)

2.1.1 Introduction of Palm Oil Processing

In palm oil mill, fresh fruit bunches (FFB) go through four main procedures to produce palm oil. During palm processing, three wastes streams are generated namely solid wastes, liquid and gaseous emissions. Rupani et al. [2010] reported the procedures of palm oil and POME production process in detail as follows. Sterilization of FFB at 140°C is the first stage in crude palm oil extraction, which aims to prevent oil hydrolysis and to loosen the palm fruits from bunches. Followed by stripping (or threshing), palm fruit is separated from bunch and become available for digestion. In digester, the fruit is mashed to break the mesocarp oil-bearing cells and then the homogeneous palm oil mash flows out. Afterwards, in palm oil extraction stage, solid and water are removed by a hydrocyclone and decanters, preliminary oil purification is done by the centrifuge and vacuum drier to produce crude palm oil , and the oil slurry is further separated and purified by a clarification system.

In the mill, the steam condensate generated in sterilization is the major portion of POME. In addition, the decanter wastewater produced in extraction stage as well as water used for washing and cleaning also plays a role. Empty fruit bunches (EFB) produced in stripping and decanter cake in extraction stage are two sources of solid waste. Besides, leaves, trunk, seed shells and fibre from the mesocarp are also within the scope of solid waste. Gaseous waste composes of steam produced from the oil extraction process in the mill.

2.1.2 Characteristics of POME

POME is a kind of hot (80-90°C), acidic, oily, brownish colloidal suspension rich in degradable organic matter. If not well treated and discharged into the environment, POME will become an important pollution source that causes depletion of oxygen in receiving water body and kills living creatures as depicted in oxygen sag curve [Mellyanawaty et al., 2018]. In POME, there is a large amount of short fibres, inorganic nutrients (Na, K, Ca, Mg, Zn, Fe, Co, Cd and Co), amino acids, free organic acid, carbohydrates and nitrogenous substances [Ahmed et al., 2015]. The characteristics of POME is highly dependent on process design, operations and quality control in the palm oil mill, thus POME composition varies in different factories and seasons [Yoochatchaval et al., 2011]. In this project, the POME produced from factories in Malaysia is specifically focused on. Table A.2 in Appendix A lists the typical characteristics of raw POME, which can be referred to make a better choice of POME treatment technology. To evaluate water treatment efficiency and regulate water reuse, Malaysian Department of Environment (DOE) published the discharge limit (Table A.4 in Appendix A) and WHO provided the guidelines for wastewater reuse (Table A.5 in Appendix A). To produce one tonne crude palm oil, 5-7.5 tonnes water is used, and averagely 3 tons of water ends up as POME [Ahmad

et al., 2003; Chin et al., 2013; Nnaji et al., 2016; Kamyab et al., 2018]. Considering the increasing trend of palm oil production every year, the huge quantity of POME attracts more attention. It was estimated that 87.8 million tonnes of POME were generated in Malaysia in 2009 and in 2017 the quantity rose to 178.9 million tonnes [Rupani et al., 2010; Ahmad and Ghufran, 2019]. On the other hand, there is a great potential of resource recovery owing to high content of oil in POME (4-15.9 g/L) and the considerable POME quantity every year [Yoochatchaval et al., 2011; Chin et al., 2013].

Apart from the composition and quantity mentioned above, other physio-chemical properties of POME are also essential for the selection of treatment technology. Zhong et al. [2013] reported that the general oil droplets size of oily wastewater in agriculture was in the range of 0.8 - 1.3 μm, which belonged to the category of emulsified oil (size <20μm) in oily wastewater. The particle size dietribution (PSD) and composition of oily water vary with time due to lipid hydrolysis. GRIT et al. [1993] took phosphatidylcholine (PHEPC, a kind of partially hydrogenated lipid in egg) as an example of lipid to study the factors affecting emulsion stability in the aspect of lipid hydrolysis extent. The results revealed the significant effect of pH, higher hydrolysis constant K_{obs} (s^{-1}) measured at very basic and acid conditions and the maximum stability occurring at pH 6.5 with lowest K_{obs}, which was shown in Figure A.3 in Appendix A. Another important factor was reported to be temperature as the relation between temperature and hydrolysis constant described by Arrhenius equation [GRIT et al., 1993]. Besides, both Zhang and Pawelchak [2000] and GRIT et al. [1993] reported the very slight effect of ionic strength on lipid hydrolysis, thus the effect of conductivity caused by pH adjustment in research and application doesn't need taking into consideration. Lek et al. [2018] and Zahrim et al. [2014] tested zeta potential of untreated raw POME produced from 2 palm oil mills located two Malaysian cities and got the results of -15.4 and -18mV, respectively. The difference of zeta potential between hot, fresh POME and POME in cooling pond didn't show much difference (<1mV), indicating the ignorable effect of temperature on the charge of oil droplets in POME. Besides, the real POME was characterized in the aspect of pH effect on zeta potential and oil droplet size in the range of pH 3 - 11, shown in Figure A.4 in Appendix A [Azmi and Omar]. Zeta potential was negative in the whole range, indicating that oil droplets in POME were always negatively charged. Oil droplet kept stable size in pH range of 3 - 10 and became larger only on at pH 11.

Like all fats, palm oil is composed of fatty acids, esterified with glycerol [Lai et al., 2015]. The fatty acids in POME comprise a variety of saturated, monounsaturated and polyunsaturated long chain fatty acid (LCFA) from C8 to C20, and C16 and C18 are the quantitatively top two types, which is shown in Table A.2 in Appendix A [Habib et al., 1997; Islam et al., 2018]. In oily water, the hydrolyzed LCFAs can be regarded as the natural surfactants, which make oil droplets surrounded by the surfactant film [Chakrabarty et al., 2008]. Table A.2 in appendix 1 list some of chemical and physical characteristics of the fatty acids in POME. pKa is the acid dissociation constant representing the strength of acid, and the larger pKa value corresponds to the weaker acid type and lower dissociation degree, which determines percentage of different existence forms (ion or molecule) of certain LCFA in POME.

2.2 MEMBRANE FILTRATION OF OIL EMULSION

Polymeric membranes have been intensively appied for wastewater treatment.PVDF membrane is the representative with the strengths of thermal and mechanical stability, microbiological resistance and higher cost-effectiveness over other polymer

materials [Asatekin et al., 2007; Hashim et al., 2009; Huang et al., 2015]. However, when treating wastwater with solutes of natural organic matter, hydrophobic PVDF membrane is susceptible to fouling due to solute adsorption on membrane and blockage of membrane pores with elongated time. Besides, due to high temperature of POME (80-90°C), polymeric membranes were not able to directly filtrate fresh and hot POME. In these studies ([Hsieh, 1996; Monash and Pugazhenthi, 2011; Zhong et al., 2013]), hydrophilic ceramic membranes were applied to treat oily wastewater treatment with high oil rejection. Great advantages of anti-fouling property, chemical and thermal stability in comparison with organic polymer membrane were reported [Hua et al., 2007; Abadi et al., 2011; Madaeni et al., 2012]. The most commonly used ceramic membranes are made from oxides such as alumina, zirconia, titania, silica and the combination of different materials that provide high permeate flux [Abadi et al., 2011; Goh and Ismail, 2018].

2.2.1 General Mechanisms of Ultrafiltration

When treating organic solutes, the rejection of solutes in UF treatment mainly attributes to steric hindrance, electrostatic interaction, hydrophobic and hydrophilic interactions [Verliefde et al., 2008]. This subsection will introduce these three filtration mechanisms. In ultrafiltration (UF) process, membrane permeability is determined by a mumbler of factors including pore size, thickness of the separating layer and the porosity of membrane. Thus to explain the mechanisms separately, sometimes it is necessary to mention the premise in advance.

Steric hindrance is strongly correlated with membrane pore size. For the same membrane with the same thickness and porosity, a smaller pore size allows for better separation ability with higher rejection rate due to stronger steric hindrance, however, it reduces permeability and accelerates fouling formation on the membrane. As Mehta and Zydney [2005] reported, all the membranes studied exhibit a similar trade-off between separation factor and permeability, that is, membranes with high separation factors will have relatively low permeability while those with high permeability have low separation factors, which is one of the limitations of current membrane technology.

Electrostatic interaction between membrane and solutes plays an important role in oil rejection and membrane anti-fouling property. The interaction, repulsion or attraction, relies on the charge of membrane and solutes. If both are negatively or positively charged, electrostatic repulsion will hinder solutes getting close to membrane surface thus decrease solute concentration near the surface of membrane surface. While the oppositely charged membrane and solutes enable electrostatic attraction between, increasing solute concentration near membrane surface. The selective retention of some constituents via influent transport that leads to the accumulation of some solutes on or near the membrane surface is denoted as concentration polarisation [Verliefde et al., 2008]. In the cases where electrostatic repulsion exists between membrane surface and solutes (or particles), high rejection rate is expected.

The hydrophilicity/hydrophobicity of the materials affects how easily the two types of materials bond together. The combination of water and hydrophilic materials is called hydrophilic interaction. Since the water targeted by the permeate is easier to bind to the hydrophilic membrane material and pass through the pores, the hydrophilic membrane has greater permeability and better anti-fouling performance. In references [Ochoa et al., 2003], commercial PVDF membranes was modified by depositing more hydrophilic substances on membrane surface. When deposition didn't significantly cause pore size reduction, both the permeability and anti-fouling property were improved due to the enhancement of membrane hydrophilicity. Zou et al. [2011] made similar changes. Although the permeability

reduction due to the side effect of plasma polymerization (a membrane modification methodology) was observed, the anti-fouling performance was still improved, owing to the increased hydrophilicity of the membrane.

The hydrophobic interaction between hydrophobic membrane and solute (or particle) contributes to their binding. The release of water molecules from two hydrophobic materials is the main driving force that enables to gain entropy due to their larger degree of freedom [Haynes and Norde, 1994]. However, the hydrophobic interaction is limited by the distance of two hydrophobic materials, which sometimes correlates to the type of electrostatic interaction between [Verliefde et al., 2008]. When the electrostatic interaction between the hydrophobic membrane and the hydrophobic solute is repulsive, the solutes (or particles) will not engage in hydrophobic interaction since they can't approach membrane surface.

2.2.2 Mechanism of Oil Emulsion Filtration: The Transformation of Surface Interactions

He et al. [2017] reported the variation of surface interaction caused by oil layer formation on the microfiltration membrane. At initial filtration stage, foulant deposition is controlled by membrane-oil droplet interaction. During filtration, driven by pressure provided in the setup, oil droplets are brought to get closer to the membrane surface, which may cause oil deposition. With sufficient oil droplet deposition and coalescence along time, an oil layer can form on the membrane surface. In this way, initial membrane-oil droplet surface interaction transform to oil layer-oil droplet surface interaction, which are often repulsive so that membrane fouling can be mitigated. In addition, He et al. [2016] pointed out that fouling propensity was directly related to foulant zeta potential that indirectly affect electrostatic interaction.

The transformation of surface interaction was also reported in the study of nanofiltration of colloidal materials and dissolved natural organic matter [Li and Elimelech, 2006], thus this theory can be possibly applied in ultrafiltration process as well. Furthermore, Tummons et al. [2016] reported a dynamic filtration process where droplet coalescence and crossflow shear controlled membrane fouling. To be specific, the transportation of oil towards membrane driven by permeate flow is balanced by the shear-induced removal of the droplets that coalesce to exceed a critical size.

2.2.3 The Effect of pH and CFV

In addition to the characteristics of membrane and solutes (or particles), the operating parameters - pH and cross-flow velocity (CFV) also significantly affect the rejection rate of pollutants and the anti-fouling performance of membrane. Under different parameter settings, not only is the fouling formation process retarded or accelerated, but the fouling/filtration mechanisms can be transformed.

Isoelectric point (IEP) is a basic parameter of a membrane, which is used to determine the type of charge on membrane surface at a specific pH. Membrane is negatively charged when pH of feed solution is above IEP and positively charged below IEP. Combined with the charge of solute (or particle), the electrostatic interaction between membrane and solutes (or particles) can be clarified, which is closely related to the retention of pollutants in the filtration process.

Chakrabarty et al. [2008] synthesized a series of polysulfone (PSf) membranes by dosing different additives and executed constant-pressure ultrafiltration experiments treating oil-in-water emulsion at pH 5, 6 and 8. The effect of pH on permeate flux was complex as the trend of flux variation was different with different membranes, and surely there's no rule to follow or conclude. For oily water ultrafiltration, apart from membrane-particle interaction and oil particle adsorption that significantly affect membrane performance, with the variation of pH, the natural surfactant, LCFA hydrolyzed from oil, possibly played a role. The natural surfactants may either reduce or increase permeate flux due to their absorptive interactions with membrane surface driven by electrostatic forces or hydrophobic effects [Byhlin and Jönsson, 2003]. For the membranes with different composition, when tested at different pH, the interaction between membrane surface and oil droplets with surrounding surfactant varied, which resulted in different flux variation trends with the variation of pH. Therefore, to investigate ultrafiltration performance of a certain membrane treating specific wastewater, it is necessary to discuss the effect of pH.

In ultrafiltration process, oil was rejected by membrane and accumulated near membrane, which generated concentration gradient that led to flux decline. Lobo et al. [2006] also reported that, in constant-pressure membrane filtration, the increase of CFV significantly improved flux when TMP was above a certain TMP value. The reason is, higher CFV could provide stronger turbulence to mitigate concentration polarization [Wu and Lee, 1999; Nabi et al., 2000]. Besides, compared with large-pore membrane (300kDa), the effect of CFV on flux of small-pore membrane (50 kDa) was more obvious, and so was the effect of CFV on oil rejection, which was possibly because of the dominance of steric hindrance and negligible charge effects for large-pore membrane [Causserand et al., 2004; Opong and Zydney, 1991].

2.2.4 Membrane Fouling Mechanism

In ultrafiltration, membrane fouling is directly attributed to pore blocking and cake layer formation caused by foulant deposition and its adsorption on membrane and pores. It was reported that the primary resistance to permeate flow was provided by the fouling layer formed on the membrane along with the membrane itself [Chakrabarty et al., 2008]. In this process, membrane-foulant and foulant-foulant interactions control fouling condition [Lee et al., 2017]. Thus, to discuss fouling mechanisms, it is necessary to identify the characteristics of both feed membrane and foulant (pollutants) in feed solution.

For feed solution, the size of solute (particle) was not found to significantly affect fouling phenomena, but the charge of it would have decisive effect on membrane-foulant electrostatic interaction (repulsion or attraction), thus the extent of foulant deposition and adsorption could be predicted [Bessiere et al., 2009; Lee et al., 2017]. Furthermore, the foulant-foulant interaction of various composition in feed solution could either enhance or reduce fouling formation. For instance, the addition of ions in protein solution may decreased foulant deposition by charge shielding effect on protein mixture; mixing of individual pollutants in one solution reduced fouling character of individual compounds [Lee et al., 2017; De Angelis and de Cortalezzi, 2013]; while in another paper [Bessiere et al., 2009], mixing of solutes significantly worsen membrane performance due to synergistic effect.

When taking oil hydrolysis into consideration, the hydrolyzed long chain fatty acids (LCFA) contribute to membrane fouling via their adsorption on membrane pore walls. Determined by pKa and the type of C-C bond respectively, the dissociation level and the shape of different LCFA are the two main factors affecting fouling

condition. Weaker acid (larger pKa) has lower ion-to-molecule ratio and are more prone to cause severer fouling owing to molecule adsorption, particularly in acidic solutions with lower acid dissociation level [Brinck et al., 2000; Amin et al., 2010; Amin and Mohammad, 2018]. In the aspect of C-C bond effect, oleic acid (18:1n9) and stearic acid (18:0) were compared, the "V" shape of oleic acid caused by the cis-double-bond functional group makes it easier to enter the membrane pores thus causing more severe membrane fouling [Amin et al., 2010]. Besides, LCFA are also regarded as natural surfactants which potentially improve the stability of oil emulsion. The surfactant concentration in oil-in-water emulsion affected its stability and membrane surface by varying quantity of surfactant molecules absorbed on oil droplets and membrane, respectively, which will be demonstrated in detail in the following Section 2.3 [Nabi et al., 2000; de Vos and Lindhoud, 2019].

For membrane, isoelectric point (IEP) and its hydrophilicity are the two main factors affecting fouling condition. The former correlates with the type and quantity of charges at different pH. When pH is around IEP value, membrane is neutral; below IEP, membrane is positively charged and the charge will be reversed when pH shifts below IEP value (Figure 2.1) [Nabi et al., 2000]. pH variation significantly affects fouling formation by transforming the type of electrostatic interaction (repulsion or attraction) between membrane and foulant, as well as increasing or reducing charges on membrane as Figure 2.1 shows. An example is provided by Lee et al. [2017], for the PES-UF membranes and protein that are negatively charged, pore blocking at the initial stage and cake layer formation at the later stage at pH 4.7 near IEP (2.9) was alleviated at pH 7.0 and 10.4 due to the increased electrostatic repulsion. Hydrophilic membrane membrane tends to have less fouling propensity, higher flux but lower fatty acid rejection compared with hydrophobic membrane [Amin et al., 2010].

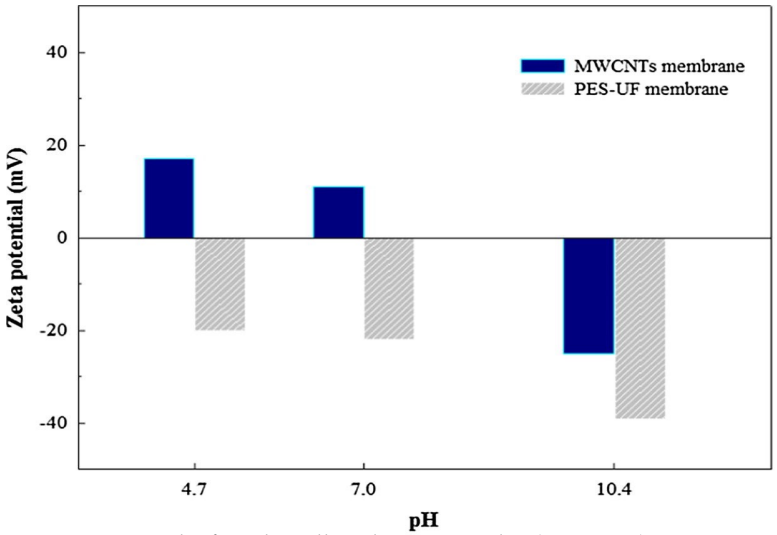

Figure 2.1: Zeta potential of multiwall carbon nanotube (MWCNT) composite membrane and commercial polyethersulfone ultrafiltration (PES-UF) membrane at different pHs (4.7, 7.0 and 10.4). (IEP_{MWCNT} = 9.2; IEP_{PES-UF} = 2.9) [Lee et al., 2017].

2.3 THE EFFECT OF SURFACTANT

To improve membrane filtration performance, especially in irreversible fouling aspects, anionic or cationic surfactants are dosed in feed oily water. Surfactant can decrease oil-water interfacial tension and modifying membrane surface property by surfactant absorption via electrostatic interaction between membrane and surfac-

tant, in which pH value plays an important role. Surfactant concentration is also an important parameter that affects membrane performance because it determines the stability of oil emulsion and the alignment of surfactant.

2.3.1 Introduction of Surfactant

Surfactant refers to a substance composed of a polar hydrophilic group and a non-polar hydrophobic group that can significantly change the interface state of the solution system by adding a small amount. The fixed hydrophilic head and lipophilic tail are able to arrange the surfactant ions on the surface of the solution or of solid material. For oil recovery, surfactant/biosurfactant pretreatment of feed solution is essential for enhancing the recovery process. Considering the potential toxicity of chemical surfactant towards environment and the inhibition of biological activity, biosurfactant is the better choice with great strengths in environmental and operational aspects such as high biodegradability, low toxicity, bio-compatibility and digestibility. According to the application of different biosurfactants provided by Usman et al. [2016], lipopeptide was found to be the best choice. However, in practice, owing to the high cost of biosurfactants (Surfactin, CAS Number 24730-31-2 (50mg) = EUR 1,090), surfactants like sodium dodecyl sulfate (SDS) are preferably and commonly used to solubilize hydrocarbon matter in oily wastewater.

Despite the least toxicity of SDS among the most widely used chemical surfactants, the inhibition of biodegradation by SDS is still worth attention. SDS is not only preferentially utilized by hydrocarbon degraders but has destructive effect on cell membrane and enzyme even for the microbes that rely on SDS as the sole carbon source [Shcherbakova et al., 1999; Cserháti et al., 2002]. SDS concentration is an important parameter determining both the filtration performance and biodegradation of mixed solution [Margesin and Schinner, 1999; Yu et al., 2007]. Shcherbakova et al. [1999] discussed the toxic effect of surfactants on methanogenesis and reported the inhibition concentrations of SDS, which were 228, 573 and 925mg/L producing 20, 50, and 80% inhibition, respectively.

2.3.2 The Effect of Surfactant on POME

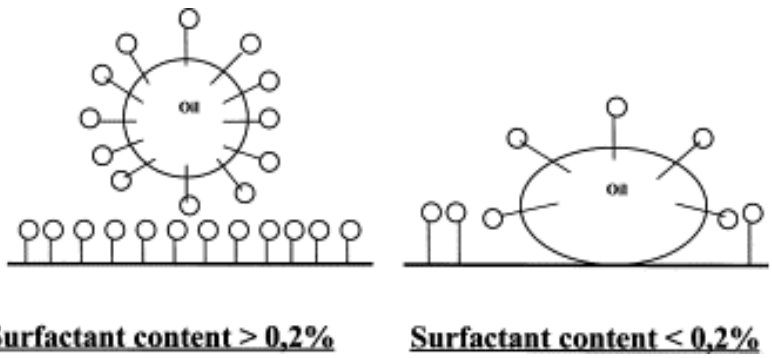

Figure 2.2: Schematic representations of the droplet deposits on hydrophobic inorganic zirconium oxide membrane (The symbol % is weight percentage w/w% of surfactant in oil emulsion) [Nabi et al., 2000].

Figure 2.2 (oil droplet in the left side) demonstrates the way of surfactant alignment on oil droplet. Lipophilic tail of a surfactant adsorbs on the surface of oil droplet via hydrophobic interaction, and the charged hydrophilic head orientates towards bulk solution via hydrophilic interaction. Moreover, the association of sur-

factant and oil increases the effective size of droplets, as well as more negative charge induced by hydrophilic head enhances the electrostatic repulsion between membrane and solutes [Kumar et al., 2008].

The concentration of surfactant has significant effect on oil emulsion stability and there's a threshold concentration for certain emulsion type. Below the threshold, the surfactant present in the solution is too little to completely surround oil droplet and to form a surfactant film (Figure 2.2, oil droplet on the right side), thus oil droplets are still able to aggregate together. The deposit phenomenon makes oil emulsion inhomogeneous and unstable.

2.3.3 The Effect of Surfactant on Membrane

The anionic surfactant-membrane interactions differentiate due to different electrostatic interactions and hydrophilic/hydrophobic interactions.

Figure 2.2 explains the positive effect of surfactant on membrane performance by ensuring system stability. For a neutral (or slightly negatively charged) ceramic membrane that is hydrophobic, sufficient SDS adsorption on membrane surface via surfactant tail-membrane hydrophobic interaction in the left picture forms a layer of surfactant, which transforms membrane surface to hydrophilic condition and prevents oil droplet depositing on membrane. While in the right picture, the emulsion is not well stabilized thus not able to avoid oil adhering on membrane due to adsorption phenomenon, coalesce, and impregnate the membrane .

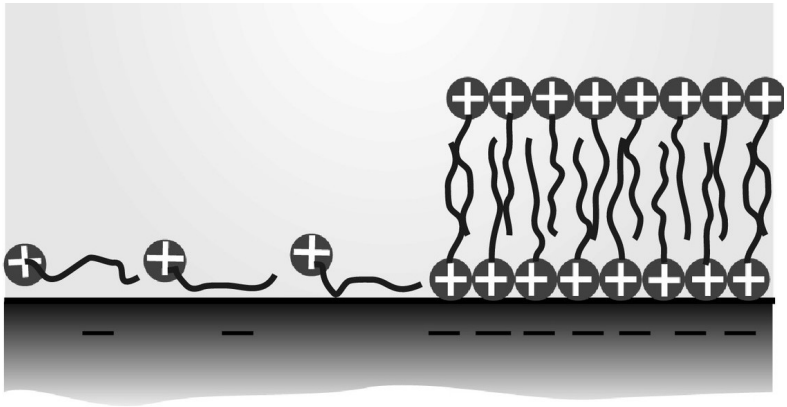

Figure 2.3: Charge inversion by Surfactant adsorption [de Vos and Lindhoud, 2019]

When the membrane surface and surfactant have adverse charges as shown in Figure 2.3, the adsorption of surfactants to the hydrophobic membrane surface leads to charge inversion. The amphiphilic nature of charged surfactant makes it arranged in two ways. One is its adsorption onto interface (Figure 2.3, left side) with surfactant tail also adsorbed on membrane via hydrophobic interaction, and head electrostatically attracted by membrane surface; the other happens when surfactant concentration above the critical micelle concentration (CMC), that is, surfactants self-assemble into micellar aggregates such as hemi-micelles or even surfactant bi-layers (Figure 2.3, right side).

Lyklema [1994] described the process of bi-layers formation in two steps. In the first step, the head of surfactant is adsorbed on oppositely charged membrane via electrostatic attraction and the extent of adsorption is determined by charge density of the interface. Then in the second step, with surfactants aggregating around the primary adsorbed species, the tail-tail hydrophobic interaction enables the second

surfactant layer neatly arranged. In this way the surfactant bi-layers are formed on membrane, reversing surface charge of membrane.

Alpha-dialumina trioxide (α-Al_2O_3) is a commonly used ceramic membrane for oily water filtration due to its higher pH_{PZC} (7.4-8.6) than titania (5.2-6.3) and zirconia(5.5-6.6), allowing slower decline of anionic surfactant adsorption capacity with increasing pH below alumina pH_{PZC} [Medina et al., 2020]. Besides, Medina et al. [2020] reported the adsorption kinetics of surfactants onto metal oxides and supported alumina over other metal oxides with less fouling potential of SDBS (sodium dodecyl benzene sulphonate) because of its smallest k/k^{-1} (adsorption rate/desorption rate) ratio compared with titania and zirconia, which represents a less organized adsorption of SDBS on alumina membrane.

2.3.4 Joint Effect of SDS in DIfferent POME Ultrafiltration Cases

To discuss the effect of surfactant on membrane performance, the focus and major surface interaction vary with different membranes. For hydrophilic polyamide membrane, Lin and Rutledge [2018] paid more attention to the hydrophilicity/hydrophobicity interaction due to the adsorption of surfactant on interface. More oleophobic membrane surface makes oil droplets hardly stay upon membrane surface and increases the likelihood of removal by shear force provided by cross flow. For hydrophobic ceramic membrane, Matos et al. [2016] focused more on electrostatic interaction between membrane and surfactant (oil droplets). Electrostatic repulsion prohibits the adsorption of surfactant (and charged oil droplets) on the membrane and its leakage across membrane pores, thus concentration polarization and cake layer formation can be reduced and permeate flux increased. Both papers gave the recommendation of more hydrophilic membrane and its charge similar to the predominant surfactant to enhance electrostatic repulsion.

However, a strong adsorption onto the membrane is normally associated with a strong passage of surfactant through membrane pores thus a higher permeate COD is obtained[Tounissou et al., 1996]. The surfactant addition increases ionic strength in feed solution, which exacerbates coagulation and compaction of cake layer and consequently reduces permeate flux at constant-pressure ultrafiltration [Matos et al., 2016]. When concentration of surfactant increases in filtration process, surfactant monomers tend to aggregate and micelles are generated near membrane surface, forming a polarization layer. The charge repulsion between negatively charged SDS micelles in the polarization layer enables presieving effect of SDS monomers thus higher retention could be obtained. Therefore, surfactant concentration in solution also alters membrane filtration mechanism and surfactant retention [Fernández et al., 2005].

3 KNOWLEDGE GAPS, RESEARCH GOALS, QUESTIONS AND HYPOTHESIS

3.1 KNOWLEDGE GAPS

1. The filtration performance, fouling condition and energy consumption of POME filtration process are unknown, thus the feasibility of direct filtration needs to be investigated.

2. For POME filtration, the membrane performances and ultrafiltration mechanisms of PVDF and α-Al_2O_3 membranes are nor clarified.

3. For POME filtration, the effects of SDS surfactant on membrane performance in the aspects of the required transmembrane pressure (TMP), process stability and permeate quality is unknown.

3.2 RESEARCH GOALS

Overarching research goal: Test the feasibility of ultrafiltration technology for POME treatment.

1. Test and compare the performance of PVDF and α-Al_2O_3 membranes for synthetic POME filtration.

2. Test the effect of permeate flux and pH on membrane performance to determine a proper operation condition and further investigate filtration mechanisms.

3. Test the function of SDS surfactant in UF process and figure out its feasibility and necessity in POME treatment.

3.3 MAIN RESEARCH QUESTIONS (RQ), HYPOTHESIS (HYP), AND SUB-QUESTIONS (SQ)

Main Research question:

Is direct membrane ultrafiltration feasible for POME treatment? What are the recovery rates of water and oil?

3.3.1 POME Synthesis

RQ1: What is the most suitable method to synthesize POME?

HyP1

POME is synthesized by mixing unrefined palm oil with demineralized water, possibly with the help of ultrasound, heating and surfactant addition methods to increase oil solubility. The synthetic POME is proven to be successfully synthesized by the comparison of oil droplet size distribution and oil concentration of synthetic POME and real POME. The synthetic POME is characterized by zeta potential at pH 2-13.

SQ1:

1) What are the size range and average size of oil droplets in synthetic POME?

2) What is the oil concentration range of synthetic POME?

3) What are the trends of zeta potential with increasing pH?

3.3.2 Membrane Performance

RQ2: How to define the optimal condition for POME ultrafiltration?

Hyp2:

1) As pore size of PVDF membrane (30nm) is much smaller than that of Al2O3 membrane (70nm), both TMP and oil rejection rate of PVDF membrane is expected to be much higher than α-Al_2O_3 membrane.

2) The fouling condition of α-Al_2O_3 membrane is far less severe than PVDF membrane due to strong repulsion between membrane and pollutants, thus merely less frequent cleaning is needed, and long lifespan can be promised.

3) The chemical cleaning of membrane shows little impact on membrane material and structure of α-Al_2O_3 membrane.

4) The operational energy consumption of α-Al_2O_3 membrane setup is lower than PVDF membrane.

SQ2:

1How is the performance (optimal flux, optimal pH, removal efficiency and anti-fouling property and stability) of PVDF and Al_2O_3 membrane for synthetic POME filtration?

2 What are the differences of filtration mechanism between two membranes?

3) What are the characteristics of permeate from membrane filtration in the steady state of the whole system? Does it meet the standards of runoff drainage or water reuse in Table I-4 of appendix I?

4) What is the optimal cleaning frequency and operating conditions that simultaneously enable good effluent quality, less energy consumption and proper membrane maintenance?

5) What's the recovery rate of POME filtration process?

6) How to describe the variation trend of TMP, rejection rate, permeate yield and quality? At which parameter state the membrane should be backwashed or chemically cleaned?

7) What is the optimal cleaning frequency and operating conditions that simultaneously enables good effluent quality, saves energy and properly maintains membrane?

3.3.3 Effect of Extra Surfactant (SDS) Pretreatment

RQ3: How is the effect of surfactant SDS on membrane performance (removal efficiency, anti-fouling property and process stability ect.)?

Hyp3:

1) The addition of SDS improves the solubility of unrefined palm oil and the stability of oil droplet size distribution.

2) The POME-SDS filtration always shows more stable TMP within each UF cycles and in continuous filtration cycles

3) As the size of SDS is much smaller than pore size of both membrane , the rejection rate of both membrane treating POME-SDS is lower than treating POME-SDS, but the addition of SDS enables less fouling.

SQ3:

1) What is the difference of rejection rate of both membranes filtrating POME and POME-SDS?

2) What is the SDS concentrations in permeate at different operation conditions?

3) At one UF cycle, does the addition of SDS make TMP variation trend more stable?

4) What is the difference of ultrafiltration mechanisms when treating no-SDS and with-SDS POME?

4 METHODOLOGY

4.1 POME SYNTHESIS AND CHARACTERIZATION

4.1.1 POME Synthesis Methodology

In this study, two kinds of palm oil mill effluent (POME), POME (without SDS) and POME with SDS (POME-SDS), were synthesized according to the following protocols based on different research objectives. According to the target oil droplet size range of 0.8 - 1.3 μm and target oil concentration of $\geq$ 4g/L, methodological parameters was determined after trials. Due to the hydrophobic interactions in oil-water mixture, hydrophobic oil tend to aggregate together and the mixture is inhomogeneous with the oil droplets or oil layer. Thus the energy-intensive Branson Digital Sonifier was needed for oil emulsification and homogenization at different energy intensity, represented as percentage of amplitude in parameter setting. The addition of surfactant SDS could lower down the energy intensity required.

1. Palm oil mill effluent without SDS (POME)

Add 6g unrefined palm oil (Brand: KTC Ltd, U.K.) a 1L bottle and fill demi-water to the 1L tick mark. Then shake the mixture at 180rpm at 55°C in New BrunswickTM Innova 40 shaker for 24 hours, followed by 30-min sonication in Sonifier at 40% amplitude. After cooling down to room temperature, sieve the mixture by using 0.103mm sieve (INTERL AB-BV) to remove solid oil aggregate.

2. Palm oil mill effluent with SDS (POME-SDS)

Add 3g unrefined palm oil and 0.3g (10% of oil mass) sodium dodecyl sulphate (SDS) (Sigma-Aldrich) to a 500mL bottle, and fill demineralized water to the 500mL tick mark. Then shake the mixture at the same condition as POME synthesis in the shaker for 24 hours, followed by 30-min sonication in Sonifier at 20% amplitude. After cooling down to room temperature, sieve the mixture by using 0.103mm sieve to remove solid oil aggregate.

When testing the effect of POME pH on membrane performance, POME was normally adjusted by using 0.1 mol/L NaOH and HCl solutions after POME synthesis procedures, except for UF at pH 2 using 37% concentrated hydrochloric acid and at pH 10 using 1mol/L NaOH solution.

4.1.2 POME Characterization and Membrane Parameters

POME was characterized by quantifying its oil concentration and clarifying other physio-chemical properties as follows. Membrane properties were also provided below.

1. COD and oil concentration

Chemical oxygen demand (COD, mg COD/L) was determined by Hach-Lange Kits. For POME, oil content (g oil/L) was directly calculated based on the tested COD value and theoretical ratio of 2.7g COD/g palm oil calculated in Appendix B.1. For POME-SDS, the SDS added in synthesis process is assumed to be completely dissolved in water, and oil concentration was calculated based on the COD value of POME-SDS minus COD caused by 600mg/L SDS addition (1208.7mg COD/L). The relationship between SDS concentrations and the corresponding COD values is shown in Appendix B.2 and the COD value of 600mg/L SDS was calculated by Equation B.4.

2. Other physico-chemical characteristics

pH was measured by Multi3430 multimeter(WTW). The size distribution of oil droplets in synthetic POME is determined by blue wave laser diffraction particle size analyzer (Civil engineering and geoscience faculty(CITG), TU Delft, NL) to compare with real POME. Zeta potential of POME-SDS (Figure 5.2 was measured by Malvern, the zeta potential analyzer(Applied Science faculty, TU Delft, NL). Literature provided zeta potential values of raw POME produced in the real palm oil mill.

3. Membrane parameters

The information of α-Al_2O_3 ceramic membrane and PVDF polymer membrane is tabulated in the Table 4.1 below.

Table 4.1: Parameters of α-Al_2O_3 and PVDF membranes.(IEP: isoelectric point)

Parameter	Brand	IEP	Inner Diameter	Pore size	Length	Cross-Sectional Area	Membrane Surface Area
Unit	-	-	mm	nm	mm	m^2	m^2
α-Al_2O_3	Inopor	8-9	7.0	70	600	3.85×10^{-7}	0.013
PVDF	Pentair	3-3.5	5.2	30	640	2.12×10^{-5}	0.010

4.2 CONSTANT-FLUX FILTRATION EXPERIMENTS WITH BACK-WASH

1. Parameter Settings of Experiments

In this study, POME were used as feed solution to investigate ultrafiltration performance of PVDF and Al_2O_3 membranes. Each membrane was tested in series at different conditions shown in Table 4.2 and 4.3 below, in which the variables were permeate flux and pH, respectively. Firstly, PVDF membrane was tested at incremental permeate fluxes with the interval of 19LMH, starting at 19LMH and increasing until the TMP exceeded the upper limit of optimal pressure range of circulation pump (<1bar). Owing to the larger pores of Al_2O_3 membrane and its hydrophilic property thus potentially higher permeability than PVDF membrane, Al_2O_3 was expected to have higher optimal flux. Thus Al_2O_3 membrane was tested starting from the optimal flux of PVDF membrane. To determine the optimal flux in the test range, three rules were considered: 1) Considering the capacity of the re-circulation pump, TMP in operation process was expected to be below 1 bar. 2) To maximize the potential of membranes treating more POME at unit duration, higher flux was preferred. 3) To reduce chemical cleaning frequency and extend membrane's lifespan, stable TMP variation and correspondingly lower irreversible fouling were expected. Then the optimal permeate fluxes for both were determined.

Table 4.2: Operational parameter setting in the experiments determining permeate permeate flux.

Parameter	pH	CFV	Permeate Flux 1	Permeate Flux 2	Permeate Flux 3
Unit	-	m/s	LMH	LMH	LMH
PVDF	5	0.78	19	38	57
α-Al_2O_3	5	0.78	38	57	76

Afterwards, the effects of pH were investigated. POME pH was adjusted to neutral condition(pH 7), below and above membrane's IEP to investigate the effects of pH, in the aspect of electrostatic interactions between membrane and oil droplets. Thus α-Al_2O_3 (IEP_{Al2O3} = 7.4-8.6) membrane was tested at pH 5 (unadjusted), 7 (neutral, below IEP) and 10 (above IEP) and PVDF (IEP_{PVDF} = 3.0- 3.5) membrane at pH 2 (below IEP), 4 (above IEP), 5 (unadjusted) and 7 (neutral). In this way, not only was the optimal conditions for ultrafiltration of both membranes were determined for subsequent long-term test, but UF mechanisms were expected to be clarified.

Table 4.3: Operational parameter setting in the experiments testing the effect of pH.

Parameter	CFV	Permeate Flux	pH 1	pH 2	pH 3	pH 4
Unit	m/s	LMH	m/s	m/s	m/s	
PVDF	0.78	38	2	4	5	7
α-Al_2O_3	0.43	28	5	7	10	-

To study the effect of SDS surfactant on membrane performance and figure out the feasibility of SDS addition, POME-SDS was also filtrated by both membranes at different conditions to compare with POME filtration performance. The operational parameters are listed in Table 4.4 and 4.5

Table 4.4: Operational parameter setting in the experiments testing the effect of SDS at different fluxes

Parameter	POME Type	CFV	pH	Permeate Flux 1	Permeate Flux 2
Unit	-	m/s	-	LMH	LMH
PVDF	POME	0.78	5	38	57
PVDF	POME-SDS	0.78	5	38	57
α-Al_2O_3	POME	0.43	5	28	42
α-Al_2O_3	POME-SDS	0.43	5	28	42

2. Operation of Cross-Flow Filtration Setup

At each condition, filtration experiment consisted of 3 cycles and 5 pure water permeability tests before and after each cycle. One filtration cycle was composed of four phases as Chen, Shang et al. (2020) stated : 1) Forward flush with feed for 15 s at a recirculation flow of 2.3L/min to fill the loop, 2) Filtration of POME(or POME-SDS) at a constant flux for 15 min, 3) Forward flush with demineralized water for 15 s at a recirculation flow of 2.3L/min to discharge concentrate, 4) Backwashing the membrane module with demineralized water at a fixed pressure of 3 bar for 1 min to remove the hydraulically reversible fouling. One permeability test was composed of 2 phases: 1) Forward flush with demineralized water for 15 sat a recirculation flow of 2.3L/min to fill the loop. 2) Filtration of demineralized water at a constant flux for 15 min. While in the long-term test, to simulate the real application process of UF, only two permeability tests of demineralized water were executed before the 1st filtration cycle and after the last cycle. No permeability test between cycles was done like short term test (3 cycles) test, but backwash was done instantly after every POME filtration cycle, which was the same as short-term test.

Table 4.5: Operational parameter setting in the experiments testing the effect of SDS at different pH

Parameter	POME Type	CFV	Permeate Flux	pH 1	pH 2	pH 3	pH 4
Unit	-	m/s	LMH	-	-		
PVDF	POME	0.78	38	2	4	5	7
PVDF	POME-SDS	0.78	38	2	4	5	7
α-Al_2O_3	POME	0.43	28	5	7	10	-
α-Al_2O_3	POME-SDS	0.43	28	5	7	10	-

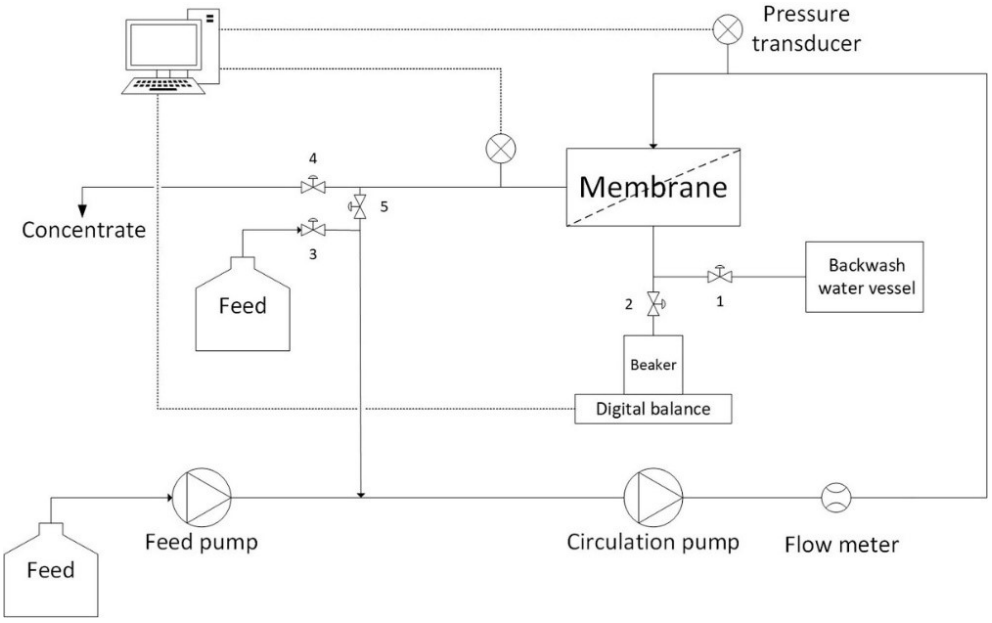

Figure 4.1: Scheme of constant-flow filtration set-up[Chen et al., 2020]

The scheme (Figure 4.1) above demonstrated the setup of filtration experiments. Table 4.6 in this section and Table C.1 in Appendix C.2 shown the operation conditions of valves and pumps. Two pumps – feed pump (DDA12-10, Grundfos, Denmark) and circulation pump (VerderGear, Verder B.V., the Netherlands) were used to dose fresh feed into circulation loop at a constant flow and provide the cross-flow velocities of 0.78m/s and 0.43m/s, monitored by the flow meter (YF-S402, Zhongjiang energy-efficient electronics Co., Itd., China). The backwash water vessel was filled with demineralized water and connected with a compressed air system to supply the fixed pressure of 3 bar for membrane backwash. Two pressure transducers were situated on two sides of membrane module and a beaker on a digital balance was set below permeate outlet of membrane. Since the pressure of the permeate stream was equal to atmospherical, the pressure exhibited by the pressure transducers was TMP [Chen et al., 2020]. The pressure transducers and balance were connected with a computer to record pressure variation and permeate weight by using DASYLab 13.0 and Kern Balance Connection software, respectively.

Table 4.6: Operation conditions of valves and pumps in the phases of filtration experiment. ("+": open/turned on, "-": closed/turned off)

No.	Phase	Valve 1	Valve 2	Valve 3	Valve 4	Valve 5	Feed Pump	Recirculation Pump
1	Forward Flush	-	+	+	+	-	-	+
2	Filtration	-	+	-	-	+	+	+
3	Forward Flush	-	+	+	+	-	-	+
4	Backwash	+	-	-	+	-	-	-

4.3 MEMBRANE PERFORMANCE EVALUATION

4.3.1 Solute Rejection Rate (Rj_i)

The rejection rate of oil or LCFA can directly evaluate the treatment efficiency of membrane, which is also a way to evaluate the electrostatic force between membrane and LCFA. Generally, stronger electrostatic repulsion corresponds to larger rejection value. Rejection rate can be calculated by the Equation 4.1 below [Verliefde et al., 2008]. The subscript i represents the rejected substance type, and $C_{p,i}$, $C_{f,i}$ are the concentrations of solute$_i$ in permeate and feed (POME or LCFA solution), respectively. In this study, the rejection rate of COD was mainly calculated and discussed, and Rj_{COD} represented rejection rate of oil since POME (without SDS) was merely composed of palm oil and water. When ultrafiltration of POME-SDS started to be discussed, COD of permeate caused by SDS and oil were roughly calculated by the methodology introduced in the following section 4.3.2, thus both oil recovery and SDS recovery could be calculated accordingly.

$$Rj_i = 1 - \frac{C_{p,i}}{C_{f,i}} \tag{4.1}$$

4.3.2 Permeate Analysis

Permeate analysis involves three parameters, COD, oil concentration and SDS concentration. COD of permeate samples is derived from 2 sources, palm oil and SDS. Overall COD value of permeate was determined by Hach-Lange Kits. For the permeate produced in POME-SDS UF process, oil concentration was roughly determined by the absorption spectroscopy of permeate samples tested by using ultraviolet–visible spectroscopy (UV-Vis) according to the relation between palm oil concentrations and corresponding absorbance shown in Appendix B.3. Then SDS concnetration can be calculated by overall COD minus COD attributing to oil dissolved in permeate and Equation B.4 in Appendix B.2.

4.3.3 Recovery Rate(R)

Because all experiments in this study were executed in constant-flux mode and Chen et al. [2020] verified that this setup (4.1) could produce permeate at constant flow as long as TMP did't encounter sharp increase, permeate flow could be regarded to be the same as feed flow at and below optimal permeate flux. Water recovery rate (R_{water}) and oil recovery rate (R_{oil}) were claculated by Equation 4.2 and 4.5, representing the ratio of permeate volume to total POME volume, and the ratio of oil weight in concentrate to that in total POME consumed in filtration process, respectively. In Equation 4.5, COD value of concentrate was determined by the equation of COD balance (Equation 4.4), in which the left and right side represent total COD involved respectively before and after one filtration cycle. However, the COD value of concentrate could not be verified by direct measurement using COD kit, because emulsified oil in feed (POME) accumulated in the cycle of the setup and formed oil droplets in concentrate, making concentrate inhomogeneous.

1). Water Recovery

$$R_{water} = \frac{Flow_{permeate}\frac{mL}{h} \times \frac{15min/cycle}{60min/h}}{Flow_{feed}\frac{mL}{h} \times \frac{15min/cycle}{60min/h} + V_{tubes} + V_{membrane}} \tag{4.2}$$

2). COD Balance:

$$Flow_{feed} \times COD_{POME} \times \frac{15\,\text{min}/cycle}{60\,\text{min}/h} + V_{tubes} \times COD_{POME} \tag{4.3}$$

$$= Flow_{permeate} \times COD_{permeate} \times \frac{15\,\text{min}/cycle}{60\,\text{min}/h} + V_{tubes} \times COD_{concentrate} \tag{4.4}$$

3). Oil recovery

$$R_{oil} = \frac{(V_{tubes} + V_{membrane}) \times COD_{concentrate}}{(Flow_{feed}\frac{mL}{h} \times \frac{15min/cycle}{60min/h} + V_{tubes} + V_{membrane}) \times COD_{POME}} \tag{4.5}$$

4.3.4 Membrane Fouling Evaluation

Xing et al. [2019] utilized resistance-in-series model to evaluate membrane fouling via membrane resistances, calculated by the Equation 4.6 - 4.10 below.

$$R_t = \frac{TMP}{\mu J} = R_m + R_r + R_{ir} \tag{4.6}$$

$$R_m = \frac{TMP_0}{\mu J} \tag{4.7}$$

$$R_t = \frac{TMP_1}{\mu J} \tag{4.8}$$

$$R_{ir} = \frac{TMP_2}{\mu J} - \frac{TMP_0}{\mu J} \tag{4.9}$$

$$R_r = R_t - R_m - R_{ir} \tag{4.10}$$

where R_t (m^{-1}) is the total resistance consisting of intrinsic membrane resistance (R_m, m^{-1}), hydraulic reversible resistance (R_r, m^{-1}) and irreversible resistance (R_{ir}, m^{-1}). TMP is the trans-membrane pressure (Pa) during filtration and J is the filtration flux (m/s). μ is the dynamic viscosity (Pa· s). R_m was determined through the permeability test of pure water before the first cycle (Equation 4.7) and the average TMP of the last 50 TMP values collected at stable state was recorded as TMP_0. R_t was calculated based on the highest filtration pressure (TMP_1) as shown in 4.8. After

backwash, the average TMP in pure water permeability test was recorded as TMP_2, and R_{ir} was determined from Equation 4.9. This resistance-in-series model could eliminate the effect of the difference of initial membrane permeability caused by insufficient chemical cleaning between different experiments, making all UF results comparable. Moreover, normally R_{ir} attracts more attention since the irreversible fouling could not be cleaned by backwash. The reversible fouling will only increase energy consumption as higher pressure is required in filtration process with higher R_r.

5 RESULTS AND DISCUSSION

5.1 POME CHARACTERIZATION

By applying POME synthesis methodology illustrated in Section 4.1.1, both POME and POME-SDS were successfully synthesized, verified by the physio-chemical properties below. To provide complete physio-chemical information for subsequent results analysis, the effect of pH on oil droplet size distribution and zeta potential were also investigated.

1. COD and Oil Concentration

As the energy intensive sonifier was applied to emulsify palm oil for POME (POME-SDS) synthesis, oil concentration in emulsion was not a certain value but in a range of 3.2-5.82 and 4.5-6.0 g oil/L, respectively for POME and POME-SDS.

2. pH, Oil Droplet Size Distribution and Zeta Potential

pH of POME was 5. The oil droplet size of synthesized POME was shown in Figure 5.1, with the size of most oil droplets around 1.538 μm. The synthesized POME-SDS (Figure A.1 in Appendix A)also had similar oil droplet size distribution and peaks. Zeta potential of POME-SDS (Figure 5.2) was -50mV and it changed in the range from -57 to -43mV at pH 2-11. Without SDS addition, zeta potential of raw POME was much higher, -15.4 and -18mV as reported in literature[Lek et al., 2018] and Zahrim et al. [2014], respectively.

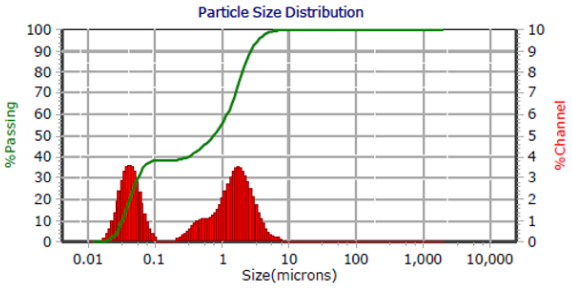

Figure 5.1: Oil droplet size distribution of POME (Peak summary: [Diameter - v/v%]: 1.538 μm - 61.5%; 0.041 μm - 38.5%).

3. Oil Droplet Size Distribution and Zeta Potential at Different pHs

When pH varied from pH 2 to pH 11, both oil droplets size distribution and zeta potential of POME (with and without SDS) changed. For POME-SDS, oil droplet size kept unchanged at pH 2-9, but the oil droplets with significantly increased size appeared at pH 10-12 (Figure A.2 in Appendix A.3). Its zeta potential fluctuated in the range from -57 to -43mV in this pH range. For POME (without SDS) tested in the referenceAzmi and Omar, with pH increasing from 2 to 11, zeta potential decreased from -10 to -35mV. Particle size variation shown the similar results as POME-SDS, that was, stable in the pH range of 3-10, and then increasing from pH 10 upwards. Besides, in this study [Azmi and Omar], zeta potential of raw POME

decreased from -10 to -35 when pH increased from 3 to 12, which was shown in Figure A.4 .

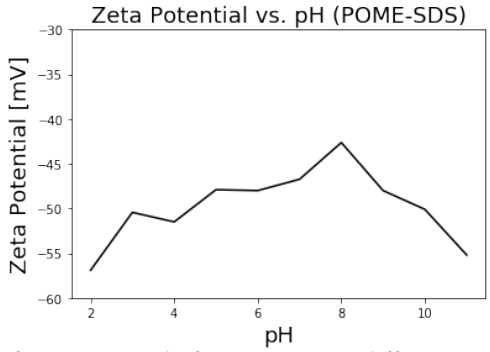

Figure 5.2: Variation of zeta potential of POME-SDS at different pH ranging from 2 to 11.

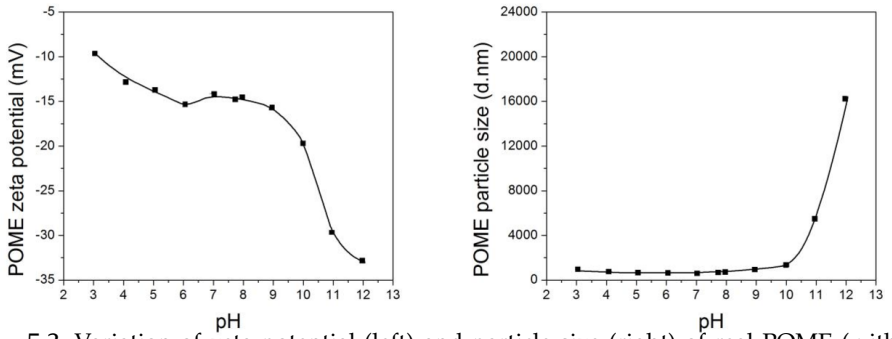

Figure 5.3: Variation of zeta potential (left) and particle size (right) of real POME (without surfactant addition) at different pH ranging from 3 to 11.Azmi and Omar

4. The Derived Information of Hydrolyzed LCFA in POME

In POME, long chain fatty acid (LCFA) is an important composition due to its function as a natural surfactant. LCFA can be hydrolyzed from oil in different conditions, including natural condition without any human intervention. In this project, the amount of hydrolyzed LCFA couldn't be directly measured, but the qualitative conclusion can be derived by other information. Due to the small extent of oil hydrolysis, the hydrolyzed LCFA in POME is not sufficient to function as a stabilizer like SDS in POME-SDS. The following paragraph explained the derivation in detail.

As palm oil is overdosed in POME-SDS preparation, the dosage of 600mg/L SDS is not redundant for the stabilization of oil emulsion, which is also proved by the decrease of oil concentration in emulsion caused by the the reduction of SDS dosage (600mg/L to 480 mg/L). Compared with the zeta potential of raw POME, more negative charges on POME-SDS indicates the inadequate LCFA in POME (without SDS) that can not completely surround oil droplet to form surfactant layer, corresponding to the accelerated oil deposit formation in less stabilized POME observed in experiments. Thus, in POME, the interaction between LCFA and oil droplets is more likely to be similar to the condition when SDS ions just surround part of the oil droplet surface (Figure 2.2, right side). While the extra dosage of chemical surfactant (SDS) will potentially make ultrafiltration system more stable, which is finally verified by the long-term test of α-Al_2O_3 membrane (Figure 5.24 in Section 5.3.3).

5.2 RESULT OF PVDF MEMBRANE ULTRAFILTRATION

PVDF membrane was firstly applied to test the feasibility of direct POME ultrafiltration. In this section, POME was firstly treated at gradient permeate fluxes, and then the experiments were executed using POME with pHs below and above IEP_{PVDF}. In this way the optimal condition (flux and pH) of PVDF membrane ultrafiltration were determined. Afterwards, POME-SDS was fed into ultrafiltration system to test the effect of extra SDS dosage on membrane performance. In the ultrafiltration process, lower TMP (at least <1bar) and less irreversible fouling were always expected.

5.2.1 Effect of Permeate Flux on PVDF Membrane Performance(TMP and Fouling)

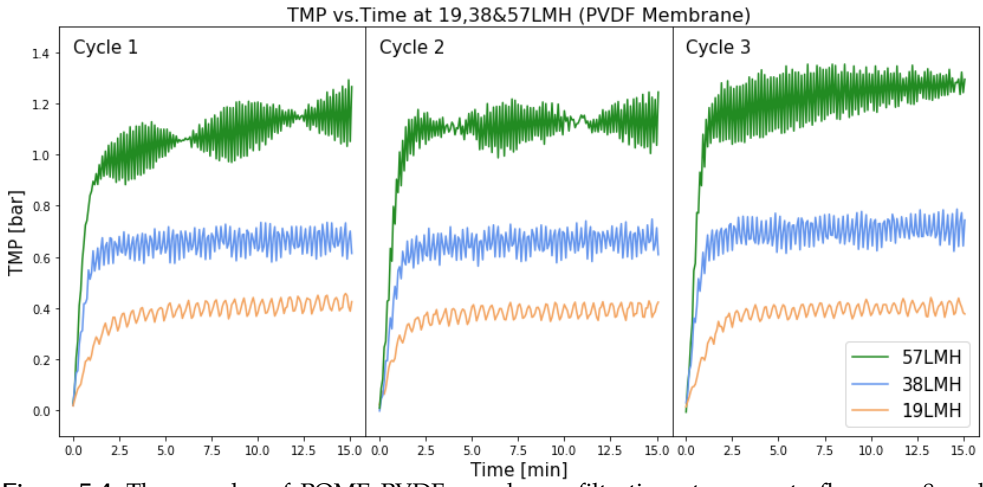

Figure 5.4: Three cycles of POME PVDF membrane filtration at permeate flux 19, 38 and 57LMH (CFV=0.78m/s).

As shown in Figure 5.4, UF of POME at gradient permeate fluxes(19, 38 and 57 LMH) determined the optimal flux at 38LMH in the test range. The condition of 38LMH allowed for lower and more stable TMP (<1 bar) compared with 57LMH, and provided higher permeate flux and similarly slight irreversible fouling compared with 19LMH (Figure 5.5). The upper limit of flux range attributed to irreversible fouling formed on the membrane that backwash was not able to remove any more.

PVDF membrane could efficiently treat POME after the 1^{st} cycle, with COD rejection rate above 99.5% and COD of permeate below 60mg/L (Figure 5.6), which met the guidelines for water discharge and reuse (Appendix A.2).

Steric hindrance and electrostatic interaction mainly functioned and resulted in stable TMP and high efficiency. The small membrane pores (30nm) guaranteed high COD rejection rate by steric hindrance. At original POME pH at 5 (above IEP_{PVDF}), the electrostatic repulsion between oil droplets (negatively charged) and PVDF membrane (negatively charged) prevented oil droplets approaching membrane surface and adsorbing onto it (Figure 5.8), thus the required TMP didn't change within each cycle and during the 3-cycle period.

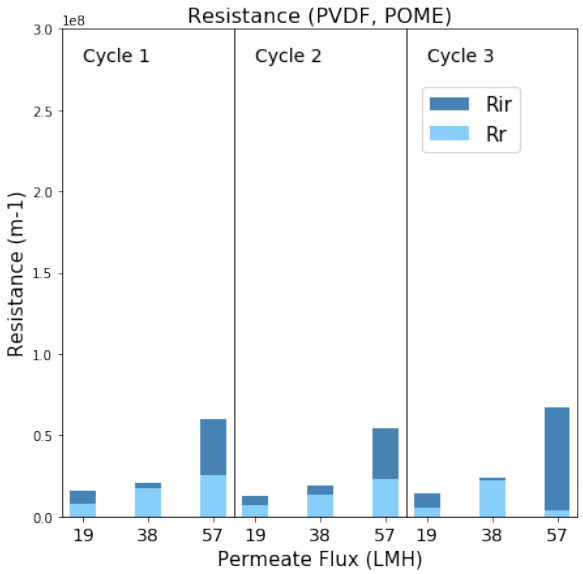

Figure 5.5: Rr and Rir variation of PVDF membrane at 19, 38 and 57 permeate flux

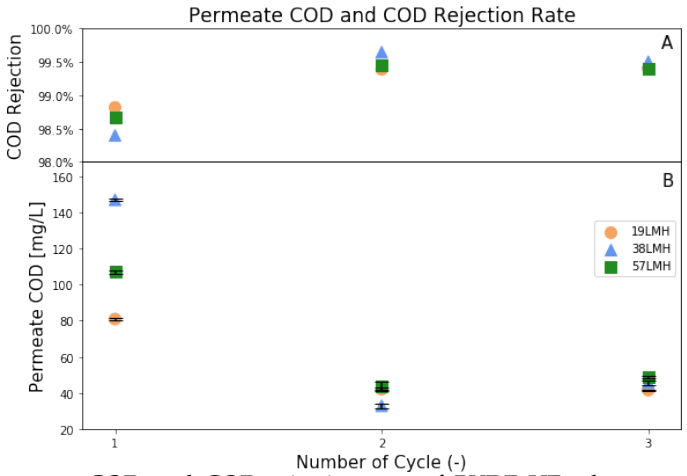

Figure 5.6: Permeate COD and COD rejection rate of PVDF UF when treating POME at CFV=0.78m/s.

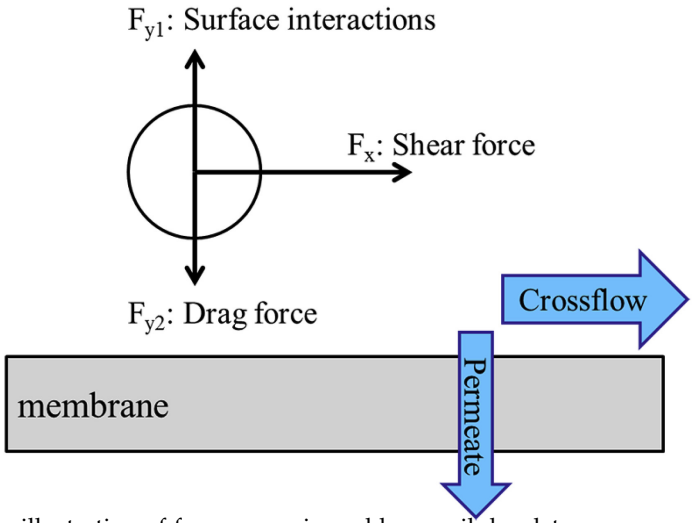

Figure 5.7: An illustration of forces experienced by an oil droplet near a membrane surface [He et al., 2017]. The x-axis is parallel to the membrane surface. The y-axis is perpendicular to the membrane surface. The shear force due to crossflow, Fx, acts in the x-direction, and the surface interactions, Fy1, and drag force, Fy2, act in the y-direction.

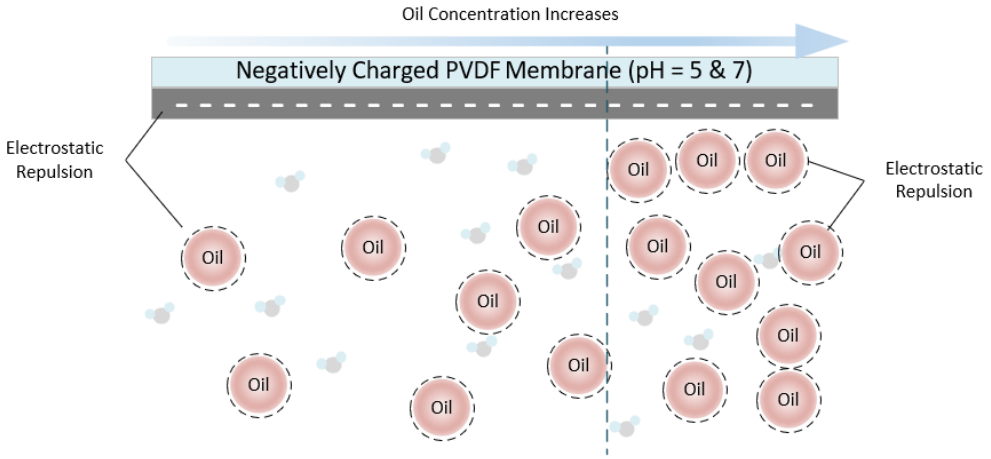

Figure 5.8: The visualized mechanism of PVDF membrane ultrafiltration of POME at pH 5 and 7 (Oil droplet-membrane repulsion and oil layer-oil droplets repulsion).

The increase of COD rejection from the 1^{st} to 2^{nd} cycle (Figure 5.6, A) could be explained by the slight fouling caused by a small amount of oil adsorbed on membrane as shown in Figure 5.8. He et al. [2017] illustrated the forces experienced by an oil droplet near a membrane by Figure 5.7. Although electrostatic repulsion significantly (F_{y1}) hindered oil droplet approaching membrane, the drag force of permeate flow (F_{y2}) controlled by pumps can lead to oil deposition on membrane. The transportation of oil towards membrane (F_{y2}) is balanced by the shear-induced removal ((F_x)) of the droplets that coalesce to exceed a critical size [He et al., 2017]. In this dynamic process, the smaller-size coalesce that was not removed by shear force played a role in the size reduction of membrane pores and the increase of COD rejection.

At higher flux (57LMH), due to severe concentration polarization near membrane, the increase of drag force compressed the layer containing large oil droplets starts forming just above the membrane surface [Chakrabarty et al., 2008], leading to the dominance of irreversible fouling as Figure 5.5 shown. In filtration process, the high pressure was not only the result of fouling formation but in turn was the driving force of compression that worsened the fouling condition. It was the synergy of oil deposition onto membrane and TMP increase that caused severe fouling.

5.2.2 The Effect of pH on PVDF Membrane Performance (TMP and Fouling)

In Figure 5.9, PVDF membrane shown apparent difference when treating POME at pH below (pH 2) and above membrane IEP (pH 5 and 7). Original POME pH was the optimal value (pH = 5).

At pH 5 and 7, negatively charged oil droplets were rejected by negatively charged membrane via electrostatic repulsion, which hindered oil adsorption onto membrane and allowed for stable TMP.

While at pH 2, the attractive force between negatively charged oil droplets and positively charged membrane made oil tightly adsorbed on membrane. The oil layer formation on a clean PVDF membrane (hydrophilic) transformed membrane surface to hydrophobic (visualized by Figure 5.10), thus membrane permeability was reduced and higher pressure was needed to maintain constant flux. Besides, drag forces (F_{y2} in Figure 5.7) provided by permeate flow and electrostatic attraction resulted in larger proportion of irreversible fouling as depicted in Figure 5.11, compared with pH 5 and 7.

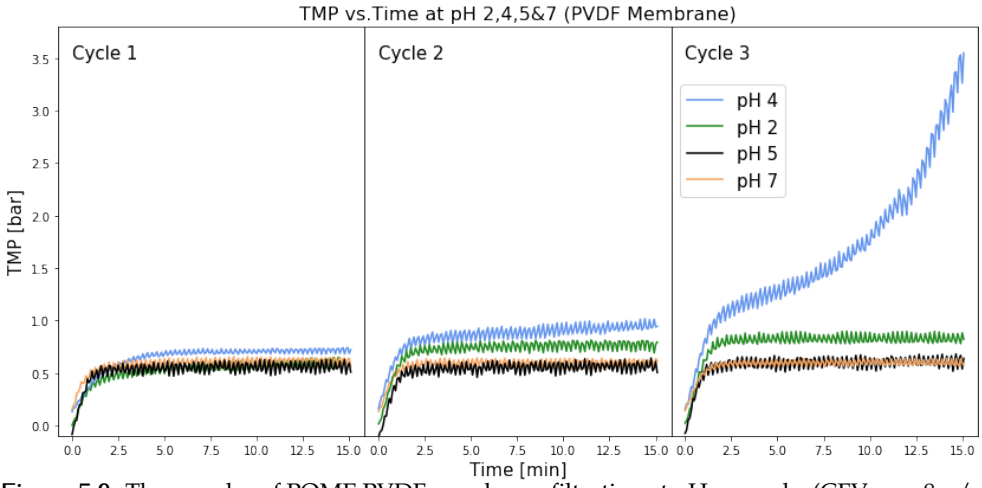

Figure 5.9: Three cycles of POME PVDF membrane filtration at pH 2,5 and 7 (CFV = 0.78m/s, Permeate Flux = 38LMH).

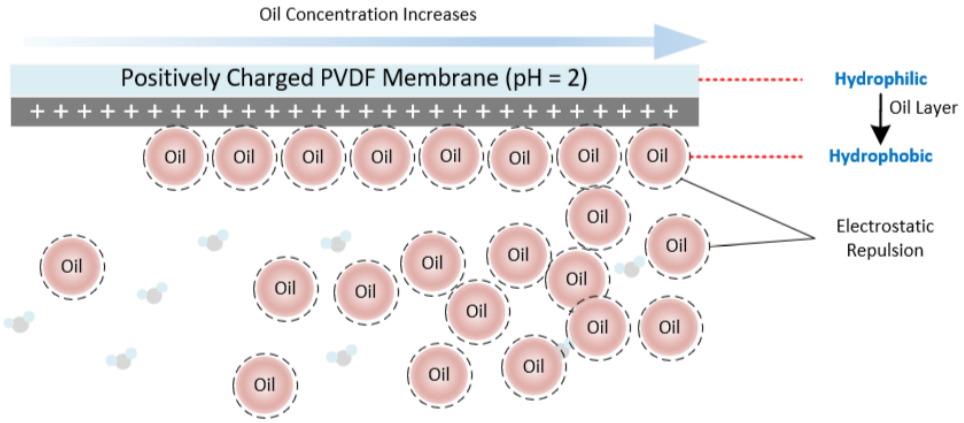

Figure 5.10: The visualized mechanism of PVDF membrane fouling at pH 2 (The change of membrane surface property caused by oil layer formation: hydrophilic to hydrophobic).

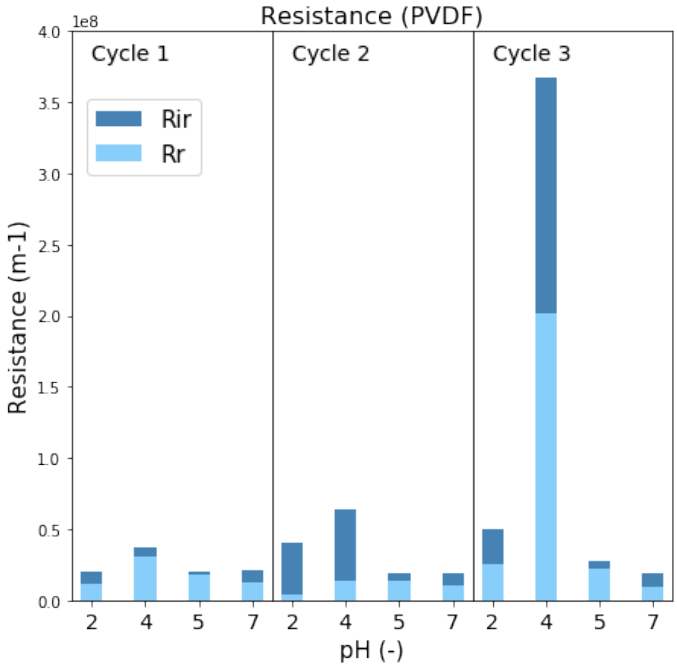

Figure 5.11: Rr and Rir variation of PVDF membrane at pH 2,4, 5 and 7.

When pH was just slightly larger than IEP_{PVDF} (pH 4), rare charges on the PVDF membrane (close to neutral state) and decreased charges of oil droplets (due to less natural surfactant ions in acidic condition), made electrostatic repulsion too weak to hinder oil adsorption and to maintain its anti-fouling property. Without the function of electrostatic repulsion (F_{y1}), the shear force provided by cross flow (F_x) was not able to sufficiently remove oil droplet coalesce on membrane. Therefore, PVDF membrane encountered gradual TMP increase from the cycle 1 to 2 and sharp increase in cycle 3 (Figure 5.9), which attributed to the synergy of oil deposition onto membrane and TMP increase demonstrated in the last paragraph of Section 5.2.1. In this process, R_{COD} also increased, from 96.5% of cycle 1 to 97.2% of cycle 2 and 98.8% of the last cycle.

5.2.3 The Effect of SDS Addition on PVDF Membrane UF Performance (Stability and Efficiency)

According to TMP variation of PVDF and resistance respectively in Figure 5.12 and 5.13, SDS addition not only didn't modify membrane performance, but caused severer fouling, especially at higher permeate flux (57LMH). Although TMP gradually decreased from cycle 1 to cycle 3 and became stable in cycle 3 at 57LMH, TMP in the test period was always above 1 bar.

In POME-SDS, SDS ions can be free or adsorbed on oil droplets to form the surfactant film (Figure 2.2, left side) as discussed in Section 2.3.2. Although more negative charges on oil droplets (and SDS) enhanced their repulsion, SDS addition increased ionic strength, which exacerbated coagulation and compaction of cake layer [Matos et al., 2016]. Besides, SDS accumulation in one filtration cycle led to the formation of a polarization layer composed of monomer aggregates and the micelles generated near membrane surface. Despite the pre-sieving effect of SDS monomers that may increase SDS rejection, the small-size SDS (molecular weight: 288.38g/mol) were prone to pass through membrane pores thus a higher permeate COD is obtained.

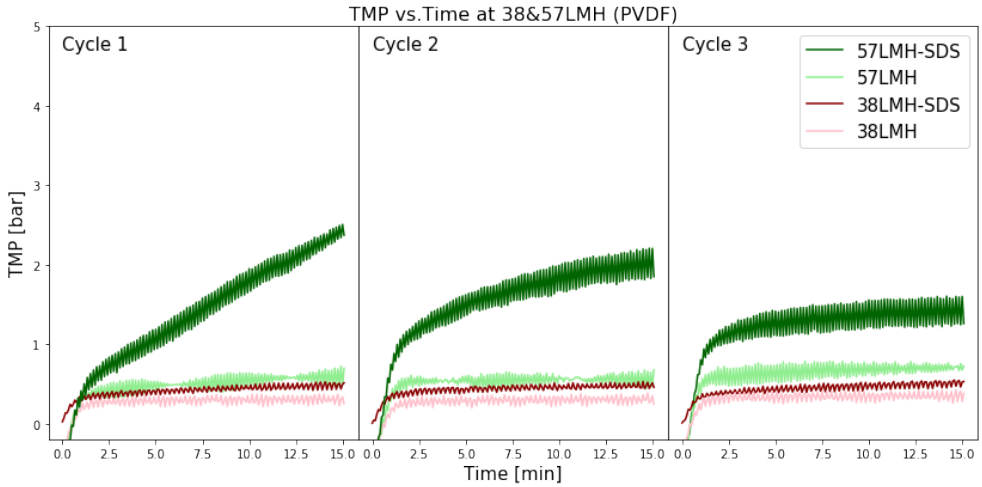

Figure 5.12: Comparison of PVDF membrane performance treating POME with and without SDS (CFV = 0.78m/s, Permeate Flux = 38 and 57LMH).

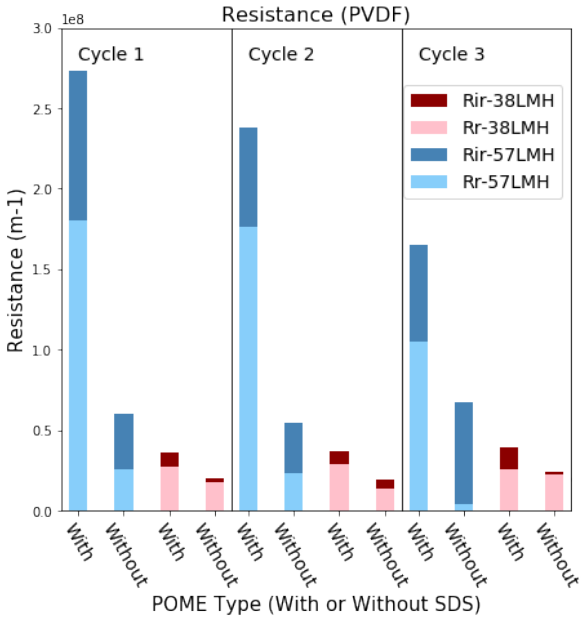

Figure 5.13: Rr and Rir variation of PVDF membrane when treating POME with and without SDS (CFV = 0.78m/s, Permeate Flux = 38 and 57 LMH).

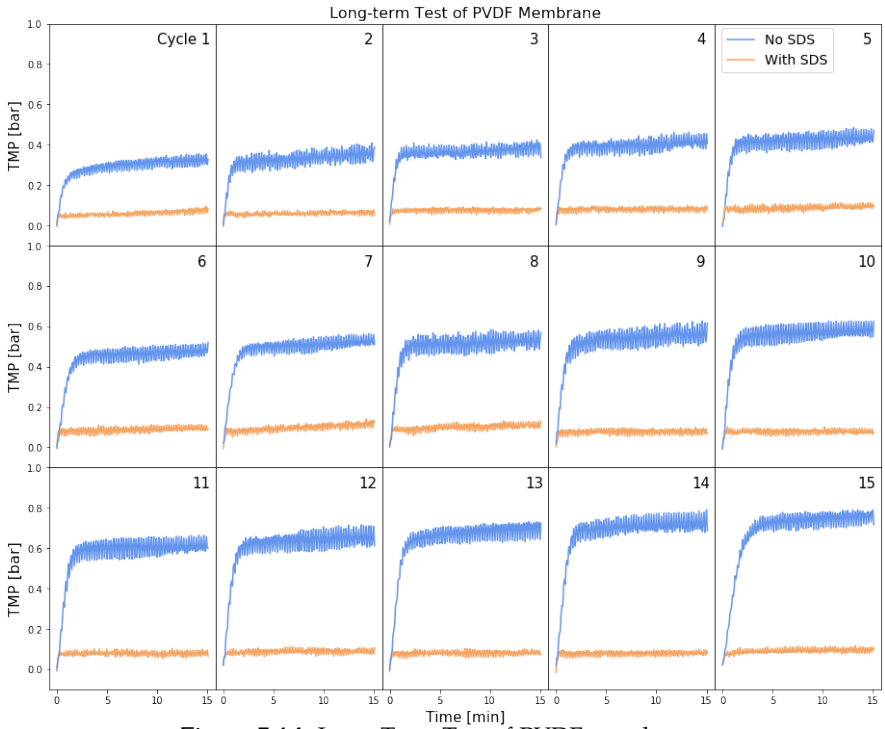

Figure 5.14: Long-Term Test of PVDF membrane.

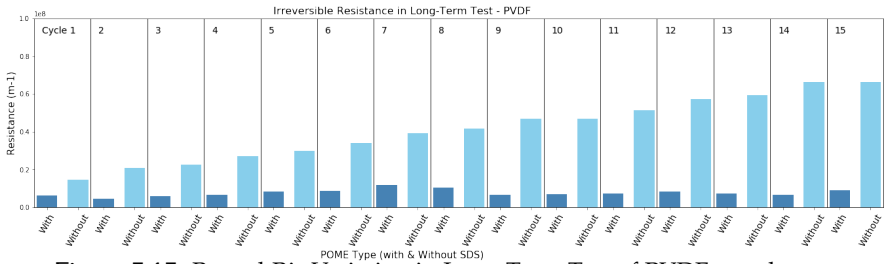

Figure 5.15: Rr and Rir Variation in Long-Term Test of PVDF membrane.

In the long-term test (TMP in Figure 5.14 and resistance in Figure 5.15), the addition of SDS in POME stabilized TMP variation. However, TMP of POME UF was always larger than POME-SDS UF, while in 3-cycle tests (Figure 5.12) shown the opposite phenomenon. The reason could possibly be that, a completely new PVDF membrane was used to execute long-term test of PVDF membrane treating POME-SDS, while the filtration of POME was done after times of filtration and chemical cleaning.

Like POME UF (without SDS) in Section 5.2.2, POME-SDS ultrafiltration was also executed at different pHs as POME and original pH (pH 5) was proved to be at the positive side with good anti-fouling performance for PVDF membranes. The results at different pH were discussed in Appendix D.1.

5.3 RESULTS OF α-AL_2O_3 MEMBRANE ULTRAFILTRATION

In this section, firstly, α-Al_2O_3 membrane was used to filtrate POME at different permeate fluxes and pHs of POME to investigate its optimal condition. Then SDS was added in POME to test the effect on membrane performance in both short-term (3 cycles) and long-term UF test. The mechanisms of oil droplet rejection and fouling formation were also discussed at each condition.

5.3.1 The Effect of Permeate Flux on α-Al_2O_3 Membrane (TMP and Fouling)

Ultrafiltration of α-Al_2O_3 membrane at different permeate fluxes started from PVDF membrane's optimal, 38LMH and subsequently increased to 57 and 76LMH. 57 LMH was α-Al_2O_3 membrane's optimal flux as depicted in Figure 5.16.

At optimal flux (57LMH), not only did α-Al_2O_3 membrane perform well with low (<0.2bar) and stable TMP within and between all cycles, but it could produce more water in unit time than at 38LMH. While at higher flux (76LMH), TMP continuously increased from the former to latter cycles and it was no longer stable within the third cycle, with an obvious increasing trend from the 12^{th} minute, which conformed to large proportion of Rir in the last cycle depicted in Figure 5.17.

The application of α-Al_2O_3 membrane in POME treatment was proved efficient with high COD rejection rates (>99.5%.) in all cycles after the 1^{st}. The increase of COD rejection at low permeate flux from the 1^{st} to 2^{nd} cycle was also observed.

The formation of oil layer on membrane surface and the reduction of pore size could explain the increase of Rj_{COD} (5.18). At original POME pH (pH 5), the electrostatic repulsion between positively charged α-Al_2O_3 membrane and negatively charged oil droplets allowed for oil adsorption and an oil layer formation on membrane, which reduced pore size and reversed membrane charge from positive to negative. The theory of charge inversion caused by foulant layer was supported by these studies [He et al., 2017; Li and Elimelech, 2006] summarised in literature review part of this report (Section 2.2.2). In this way the foulant layer formation shifted oil droplet-membrane interaction to oil droplet-oil layer interaction, and the force transformed from attractive to repulsive, hindering further adsorption of oil droplets.

Furthermore, two evidence can verify the oil layer formation theory proposed in last paragraph. The first was the high COD rejection occurring at the condition with inadequate steric hindrance (38.5% oil droplets around 46nm, <70nm of pore size) and non-beneficial oil droplets-membrane interaction (attraction). Thus the change of membrane surface happened and the formation of oil layer was reasonable. Besides, the dominance of large oil droplets (61.5%) oil droplets around 1.53mum, >70nm of pore size) make oil droplets more likely to (partly) cover membrane pores rather than adsorption into pore walls, which could prevent the formation of too much fouling caused by oil layer.

The other evidence was provided by an extra POME ultrafiltration test at lower permeate flux (14LMH) and CFV (4.3m/s) (see in Appendix C), which aimed to slow down the oil layer formation process. The gradual increase of COD rejection rate (61.4%, 86.6% and 98.5% in the 1^{st}, 2^{nd} and 3^{rd} cycle, respectively) conformed the condition of the slow formation of oil layer and further verifies the theory of oil layer formation.

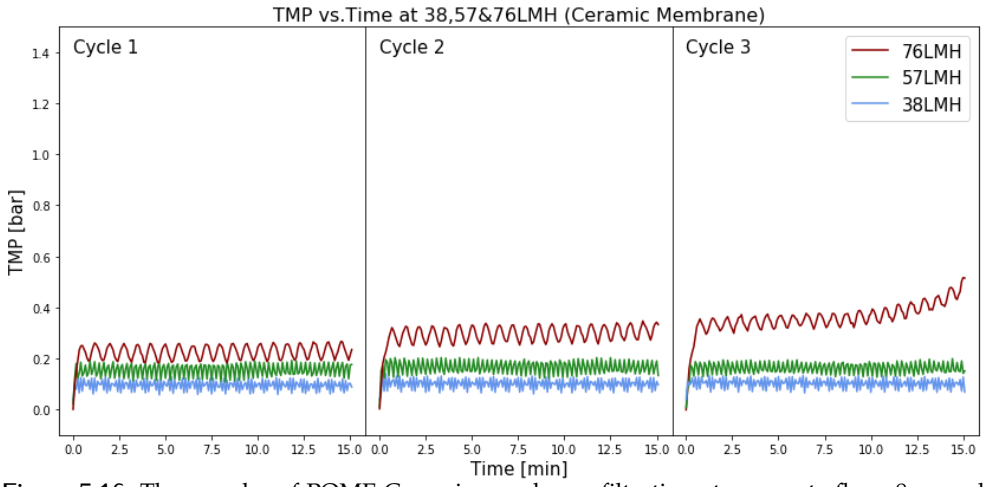

Figure 5.16: Three cycles of POME Ceramic membrane filtration at permeate flux 38,19 and 57LMH (CFV=0.78m/s).

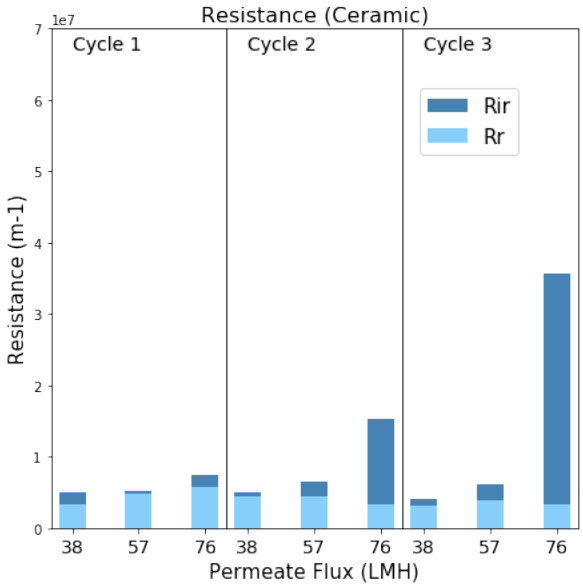

Figure 5.17: Rr and Rir variation of α-Al_2O_3 membrane at 19, 38 and 57 permeate flux

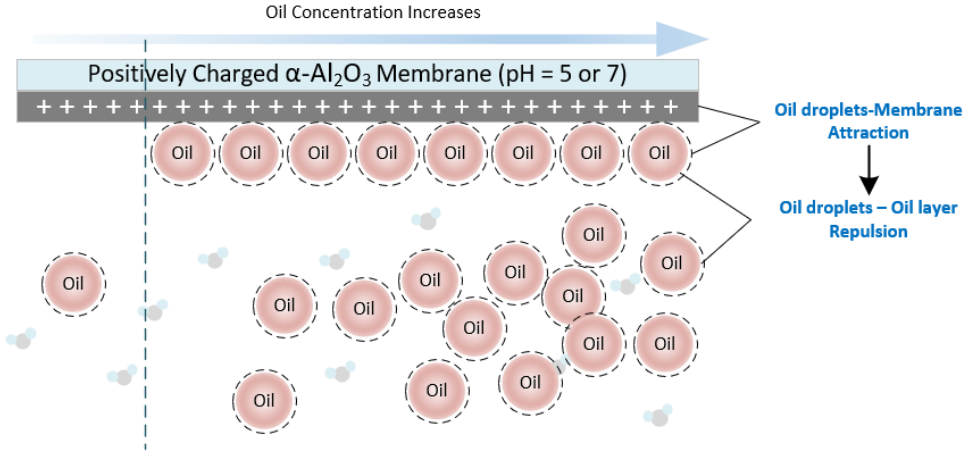

Figure 5.18: The visualized mechanism of good α-Al_2O_3 membrane performance due to charge inversion resulted from oil layer formation at pH 5 and 7.

5.3.2 The Effect of pH on α-Al_2O_3 Membrane Performance (TMP and Fouling)

In Figure 5.19, α-Al_2O_3 membrane shown apparent difference when treating POME at pH below and above membrane IEP. Fortunately, pH 5 was still in the positive side with good anti-fouling property like PVDF membrane.

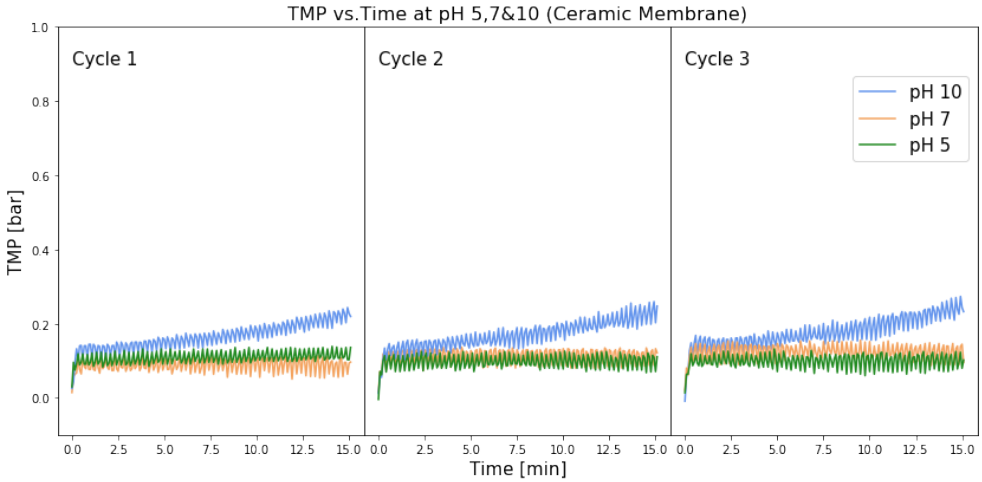

Figure 5.19: Three cycles of POME α-Al_2O_3 membrane filtration at pH 5,7 and 10 (CFV = 0.43m/s, Permeate Flux = 28LMH).

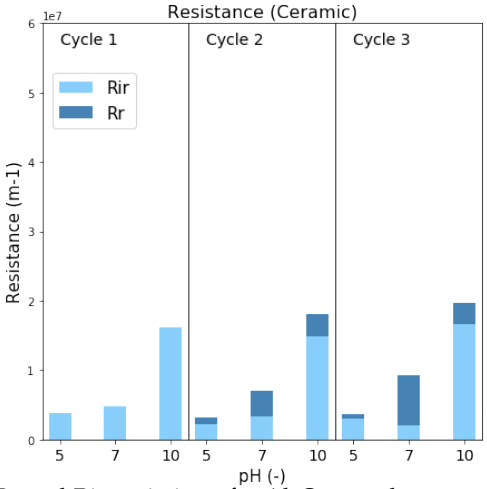

Figure 5.20: Rr and Rir variation of α-Al_2O_3 membrane at pH 5,7 and 10

α-Al_2O_3 membrane shown the opposite condition from PVDF. Below IEP_{Al2O3}, α-Al_2O_3 membrane shown stable TMP (Figure 5.19) and slight fouling (Figure 5.20), which attributed to the formation of the oil layer (5.18) and its effects on charge inversion as demonstrated in the last Section

At pH 10 above IEP_{Al2O3}, membrane performance became worse, in the aspects of climbing TMP in each cycle (Figure 5.19, blue curve) and lower Rj_{COD} values (92.2%, 97.2%, 97.4% respectively in cycle 1, 2 and 3) compared with pH 5 and 7 (98.7%, >99.5%, >99.5%). The membrane fouling at pH 10 could be possibly due to the change of solute composition caused by enhanced lipid hydrolysis and fatty acid dissociation at higher pH [GRIT et al., 1993]. Although the dissociated LCFA was likely to enable strong repulsion between negatively charged solutes and negatively charged PVDF membrane, the smaller-size components such as glycerol and LCFA ions generated in lipid hydrolysis process tended to pass through membrane pores, resulting in membrane fouling and higher COD of permeate. During pH adjustment process using 1 mol/L NaOH solution, re-dissolution (disappearance)

of small residual oil aggregates floating on POME was observed, which could verify the hypothesis above.

5.3.3 The Effect of SDS Addition on α-Al_2O_3 Membrane Performance (Stability and Efficiency)

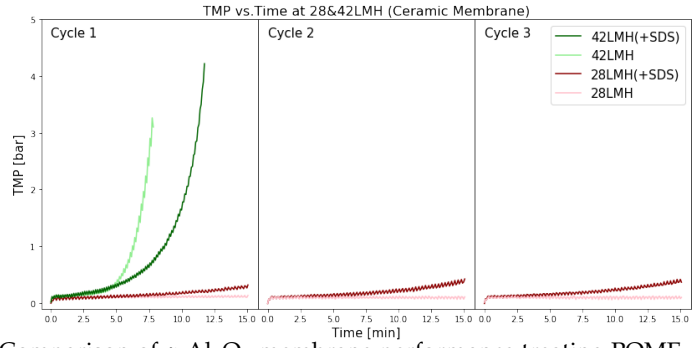

Figure 5.21: Comparison of α-Al_2O_3 membrane performance treating POME with and without SDS (CFV = 0.43m/s, Permeate Flux = 28 and 42LMH).

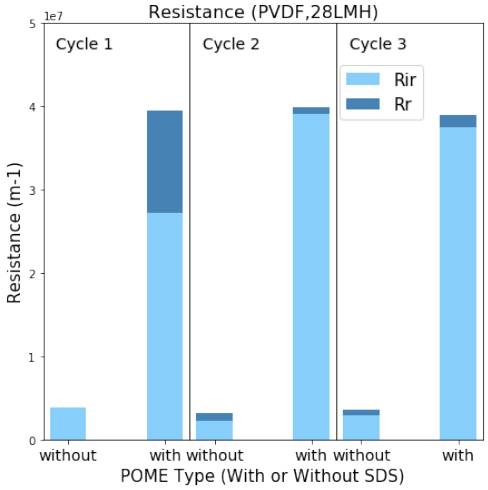

Figure 5.22: Rr and Rir variation of Ceramic membrane treating POME with and without SDS (CFV = 0.43m/s, Permeate Flux = 28LMH).

From Figure 5.21, SDS addition didn't significantly improve membrane performance by decreasing the required pressure, however the 3-cycle filtration test indicated its potential of process stabilization. By comparing the light green-light red gap (without SDS, larger) and dark green-dark red gap (with SDS, smaller), SDS mitigated TMP increase caused by flux increase, despite the fouling increment at 28LMH due to the extra pollutant (SDS) brought into feed emulsion.

The mechanism of SDS functioning in α-Al_2O_3 membrane ultrafiltration was explained by the bi-layers SDS formation on membrane surface demonstrated in Section 2.3.3 of literature review as de Vos and Lindhoud [2019] reported. Firstly, the SDS head-membrane electrostatic attraction and the SDS tail-membrane hydrophobic interaction enabled the formation of the first layer of SDS on the membrane. Afterwards, with SDS concentration increased near membrane surface, SDS ions of the second layer were neatly arranged on the first SDS layer via the SDS tail-SDS tail hydrophobic interaction, with hydrophilic head orientating towards bulk solution. In this way, the bi-layers of SDS formed on membrane. The double layers on the one hand made α-Al_2O_3 membrane become hydrophilic, thus membrane permeability was expected to be improved. On the other hand, bi-layers of SDS reversed

the charge of membrane surface to negative, the electrostatic repulsion between bi-layers and oil droplets could hinder the adsorption of oil droplets and the formation of more fouling. Nevertheless, the weaknesses of SDS dosage were also worthy of attention. The extra foulant (SDS) increase reversible fouling (Figure 5.22, cycle 2 and 3).

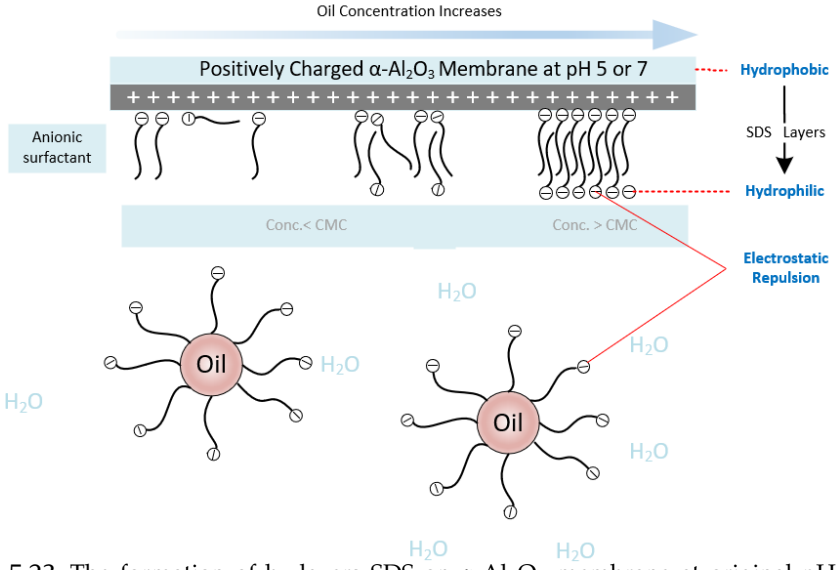

Figure 5.23: The formation of by-layers SDS on α-Al_2O_3 membrane at original pH (pH 5) and pH 7 [de Vos and Lindhoud, 2019].

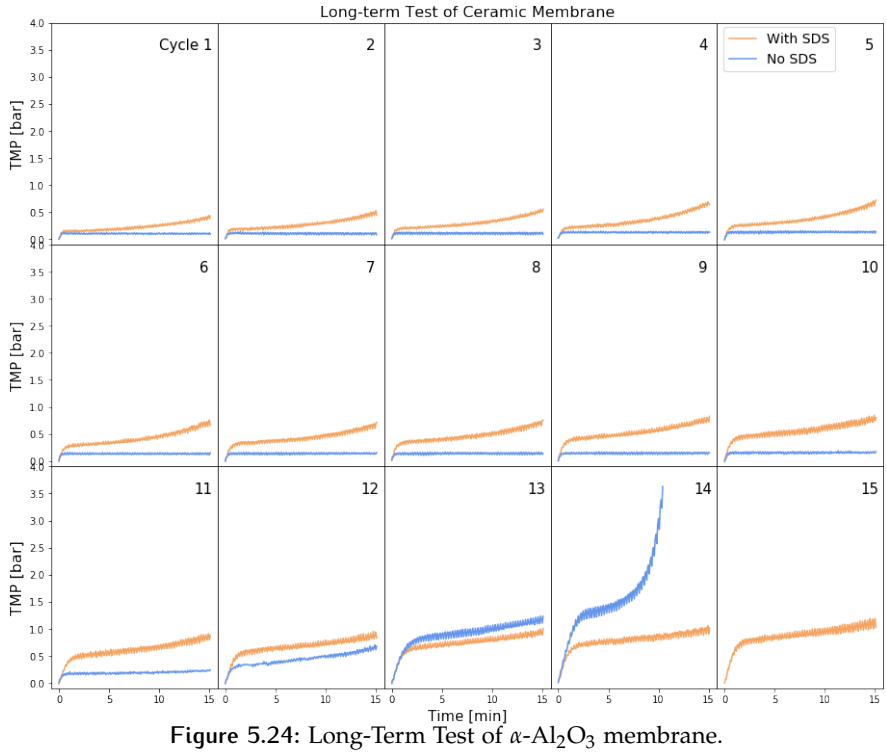

Figure 5.24: Long-Term Test of α-Al_2O_3 membrane.

The subsequent long-term test of α-Al_2O_3 membrane treating POME and POME-SDS proved SDS potential of process stabilization. In Figure 5.24, although in the first 12 cycles, the addition of SDS in UF resulted in higher TMP, in the long run (15 cycles), TMP steadily climbed within each cycle and slightly increased from former to latter cycle, which indicated the effect of SDS - retarding TMP increase and avoiding such sharp TMP increase as shown in the 14^{th} cycle of POME (without SDS) ultrafiltration. Hence, the advantages and disadvantages of SDS addition could be clarified, that is, bringing in extra fouling due to 2-layer SDS formation but "protecting" membrane from oil adsorption thus stabilizing UF process in the long run.

Ultrafiltration of POME-SDS was executed not only at different permeate fluxes, but at different pHs. The addition of SDS didn't change the effect of pH on α-Al_2O_3 membrane performance. The discussion in detail can be found in Appendix D.2.

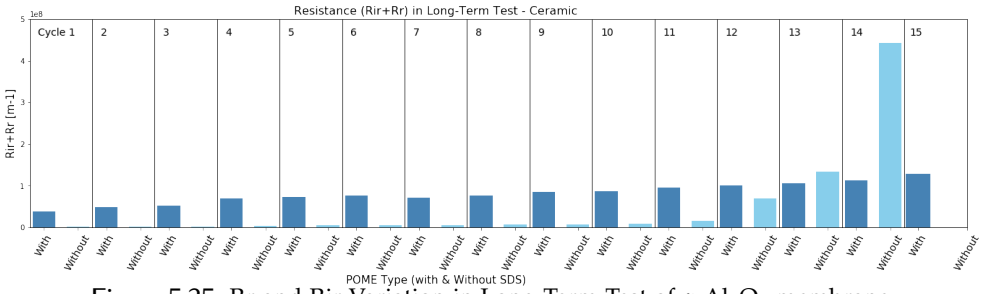

Figure 5.25: Rr and Rir Variation in Long-Term Test of α-Al_2O_3 membrane.

5.4 COMPARISON OF α-AL_2O_3 AND PVDF MEMBRANE ULTRAFILTRATION PERFORMANCE

5.4.1 Efficiency Comparison between α-Al_2O_3 and PVDF Membranes

In the aspect of POME treatment efficiency, both membranes showed quite excellent performance, with COD rejection rate higher than 99.4% in most cycles. With the addition of SDS, the low SDS rejection rate (around 40%) of both membranes worsened permeate quality. These messages were visualized by the Figure 5.26 and discussed in detail in the following paragraphs. Table 5.1 summarized the information of permeate COD and rejection values of ultrafiltration processes using the two membranes.

Table 5.1: Rejection ranges of oil and SDS respectively for PVDF and α-Al_2O_3 membranes

Membrane Type	COD_{oil}	COD_{SDS}	Rj_{oil}	Rj_{SDS}
	mg COD/L	mg COD/L	%	%
PVDF	30.7 - 42.6	796.0 - 857.6	99.6 - 99.7	29.0 - 34.1
	(One outlier: 311.4)		(One outlier: 97.3)	(One outlier: 36.6)
α-Al_2O_3	20.2 - 30.7	719.0 - 739.4	99.7 - 99.8	38.8 - 40.5

Figure 5.26 shown the variation of permeate COD from feed to cycle 1-14 (15). For POME (without SDS, left side of Figure 5.26) filtration, R_{COD} kept quite low in the whole filtration period for both membrane, while with the addition of SDS, permeate COD increased 10 times more than that of POME-SDS filtration. Beside, despite the variation of TMP and fouling formation along the whole filtration process, permeate COD was always stable for both membrane, which promise great treatment quality and stability in the long run. When treating POME-SDS, COD

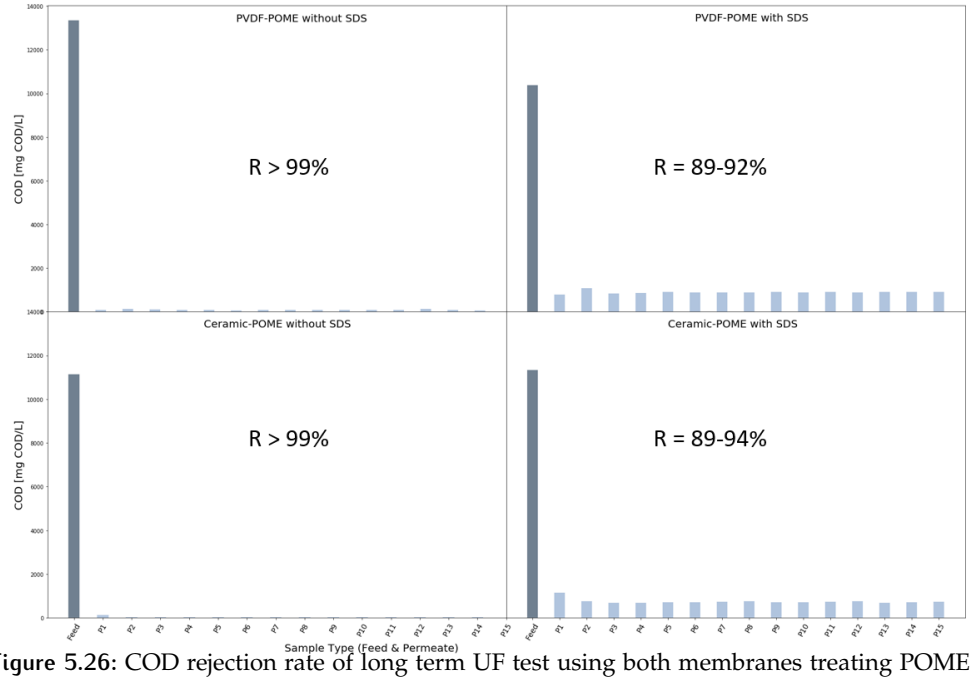

Figure 5.26: COD rejection rate of long term UF test using both membranes treating POME and POME-SDS (upper left: PVDF - POME; upper right: PVDF - POME-SDS; lower left: α-Al_2O_3 - POME; α-Al_2O_3 - POME-SDS)

value attributed to oil in permeate were determined according to the methodology as Section 4.3.2 explained. Thus COD_{SDS} as well as oil and SDS rejection rates were calculated as Table 5.1 shown. Oil rejection rate maintained around 99.7% for both membranes as in POME (without SDS) filtration process. The enhancement of oil droplet retention caused by SDS layer in POME-SDS filtration and by oil layer in POME synthesis was the same. However, SDS rejection was rather low, in the range of 29 - 34.1% and 38.8 - 40.5% for PVDF and α-Al_2O_3 membranes, respectively. The lower SDS rejection rate of α-Al_2O_3 membrane could attributed to SDS adsorptions and larger pore size (70nm) than PVDF membrane (30nm), allowing SDS passing through membrane pores more easily. Within each filtration cycle, the maximum SDS concentration in concentrate side was below 1.1 g/L (calculated based on the water recovery rate at 38LMH and the assumption of 100% SDS retention). Since the the SDS micelle radius in 2.88-144.2 mol/L SDS solution shown was in the range of 1.82 - 1.85 nm [Duplatre et al., 1996], the radius in filtration concentrate side was smaller than 1.82nm, as well as smaller than oil droplets and membrane pore size, which could explain the lower rejection rate of SDS.

5.4.2 Recovery Comparison between α-Al_2O_3 and PVDF Membranes

In ultrafiltration process, apart from the geometric parameters of membrane, the recovery of water and oil was largely determined by permeate flux. The recovery rates of oil and water were calculated by using the methodology and equations in Section 4.3.3, and the rate at different fluxes were shown in Table 5.2.

α-Al_2O_3 membrane shown great potential of higher oil recovery and more permeate production.. Its Higher optimal flux (57LMH) largely determined its higher water recover rate (62.4%) and higher concentration of oil concentration (9.5%) in concentrate. However, since the geometric parameters of two membranes were different as 4.1 shown, especially for inner diameter and pore size, the comparison of recovery between two membranes in this paragraph couldn't represent the category

of two membranes, and it was merely limited in the two membranes used in this study.

Table 5.2: Water recovery rate and oil concentration in concentrate side at different test fluxes.

Membrane Type.	Flux (LMH)	Water Recovery (%)	Oil Concentration (g/L)
PVDF	19	29.3	4.9
	38	45.3	6.4
	57	55.4	8.0
α-Al_2O_3	38	52.5	7.4
	57	62.4	9.5
	76	68.8	11.6

5.4.3 Summary of Ultrafiltration Mechanisms for α-Al_2O_3 and PVDF membranes

In this section, the mechanisms of POME ultrafiltration using α-Al_2O_3 and PVDF membranes at different conditions were summarized in the Table 5.3. Besides, the different effects of oil layer formation for the two membranes were discussed in detail in the following paragraphs.

Table 5.3: The summary of ultrafiltration mechanisms of α-Al_2O_3 and PVDF membranes at different conditions

Membrane Type.	POME Type	pH	Membrane-oil droplets electrostatic interaction	Hydrophobicity/ Hydrophilicity of clean membrane	Oil/SDS layer Formation	Membrane-new layer electrostatic interaction	Hydrophobicity /Hydrophilicity of fouled membrane surface	Membrane performance (main mechanism)
PVDF	POME	2	Attraction	hydrophilic	oil layer (neatly arranged)	Repulsion	Hydrophobic	Severe Fouling (Increased hydrophobicity of membrane surface)
	POME	4	Repulsion (very weak)	hydrophilic	Oil layer (gradually formed)	Repulsion	Hydrophobic	Severe Fouling (Oil deposition and accumulation)
	POME	5&7	Repulsion	hydrophilic	oil layer (loose)	Repulsion	Hydrophobic	Stable TMP&little fouling (membrane-oil droplet repulsion)
	POME-SDS	5	Repulsion (stronger)	hydrophilic	oil+SDS layer (loose)	Repulsion	Hydrophobic	Slightly increasing TMP, Little fouling (Membrane-oil droplet/SDS repulsion)
α-Al_2O_3	POME	5&7	Attraction	hydrophobic	oil layer (neatly arranged)	Repulsion	Hydrophobic	Stable TMP&little fouling (Charge inversion and membrane-oil droplet repulsion)
	POME	10	Repulsion	hydrophobic	oil layer (loose)	Repulsion	Hydrophobic	Severe Fouling (Deposition of Oil, & LCFA and glycerol)
	POME-SDS	5	Attraction (stronger)	hydrophobic	Bi-layers SDS (neatly arranged)	Repulsion	Hydrophilic	Slightly increasing TMP, more stable process (Charge inversion and increased hydrophilcity of membrane surface)

When membrane and oil droplet were oppositely charged, oil droplets were adsorbed on membrane and an oil layer formed on membrane surface. However, at this condition, α-Al_2O_3 membrane (pH 5 or 7) shown the opposite condition from PVDF (pH 2), with the former showing stable and good anti-fouling performance and the latter severely fouled. Despite pH effect on oil hydrolysis (enhanced) and LCFA dissociation (weakened) at pH 2 - the increased fouling likelihood of PVDF membrane was caused by more LCFA molecules (less LCFA ions in comparison), the difference of the property between two membranes also played an important role.

For hydrophilic PVDF membrane, oil layer formation transformed its surface to hydrophobic, which significantly reduced the permeability of PVDF membrane. However, in this study, the hydrophobicity of α-Al_2O_3 membrane did not change with oil layer formation. It was the destruction of the strength of a membrane

(hydrophilicity of PVDF) that significantly weakened membrane anti-fouling performance.

The different focuses of foulant deposits-foulant interaction between hydrophilic polyamide membrane Lin and Rutledge [2018] and hydrophobic ceramic membrane Matos et al. [2016] summarized in Section 2.3.3 in literature review can support the difference of oil layer formation on the two membranes and the mechanisms demonstrated in this study.

To discuss the effect of surfactant on membrane performance, the focus and major surface interaction vary with different membranes. For hydrophilic polyamide membrane, Lin and Rutledge [2018] paid more attention to the hydrophilicity/hydrophobicity interaction due to the adsorption of surfactant on interface. More oleophobic membrane surface makes oil droplets hardly stay upon membrane surface and increases the likelihood of removal by shear force provided by cross flow. For hydrophobic ceramic membrane, Matos et al. [2016] focused more on electrostatic interaction between membrane and surfactant (oil droplets).

6 CONCLUSION AND OUTLOOK

6.1 CONCLUSION

The conclusions for the research questions are given as follows:

Main Research Question: Is direct membrane ultrafiltration feasible for POME treatment? What are the recovery rates of water and oil.

Overall conclusion: Direct membrane ultrafiltration of POME is a feasible method for POME treatment with high-quality permeate and acceptable recovery rate.

1) How to define the methodology for POME synthesis?

Conclusion 1: POME was successfully synthesized by the methodology of mixing heating at 55 °C) and sonication at 40% amplitude with the dosage of 6g/L unrefined palm oil. Oil concentration in the range of 3.2-5.82 g oil/L and the size of most oil droplets around 1.54μm. The addition of SDS could enhance emulsification of oil thus increase palm oil solubility and zeta potential of POME, and reduce the energy intensity needed for POME-SDS synthesis. Oil droplets in POME and POME-SDS were always negatively charged and zeta potential of both feed was relatively stable with the variation span around 10mV.

2) How to define the optimal condition for POME ultrafiltration?

α-Al_2O_3 could provide higher permeate flux (57LMH) than PVDF membrane (38LMH). Both membranes shown obvious difference of membrane anti-fouling property below and above membrane's IEP and great membrane performance lied in at the side of original POME pH (pH 5). TMP and resistance (Rr + Rir) of α-Al_2O_3 UF was lower than PVDF membrane. Despite the pore size difference between α-Al_2O_3 (70nm) and PVDF (30nm) membranes, both membranes were efficient for oil separation with oil rejection rate higher than 99.4% expect for cycle 1. Due to oil layer formation and pore size reduction, the rejection increase was observed for both membrane from cycle one to cycle 2. The water recovery of α-Al_2O_3 membrane (62.4%) was higher than PVDF membrane (45.3%) at their optimal flux, so as the oil recovery rate of the two membranes.

At optimal POME pH (pH 5), the good anti-fouling performance of the two membranes differentiates. Charge inversion due to oil layer formation on α-Al_2O_3 membrane allowed for oil layer-oil droplets repulsion that prevented further adsorption of oil droplets onto membrane and maintained stable TMP. PVDF membrane predominantly relied on electrostatic repulsion between negatively charged membrane and negatively charged oil droplets. A thin and loose oil layer could also formed on PVDF membrane due to oil accumulation that enhanced oil rejection.

3) How is the effect of surfactant SDS on membrane performance (removal efficiency, anti-fouling property and UF stability)?

As SDS molecule size was smaller than oil droplets, the addition of SDS in POME lowered down separation efficiencies of α-Al_2O_3 and PVDF membranes to around 93% and 95%, respectively. The membrane with larger pores was more significantly

affected. Beside, SDS was an extra fouling for both membrane, thus slightly increased TMP and resistance.

For α-Al_2O_3 membrane, SDS had the potential of "protecting" membrane surface by forming bi-layers SDS on membrane surface via membrane-SDS head electrostatic attraction and SDS tail-SDS-tail hydrophobic interaction. As the results of the formation of bi-layers, charge inversion enabled SDS layer-oil droplets repulsive interaction thus avoiding oil adsorption onto membrane and originally hydrophobic α-Al_2O_3 membrane turn to be hydrophilic, allowing for higher membrane permeability. The long-term test of α-Al_2O_3 membrane proved the function of filtration process stabilization and anti-fouling property modification in the long run. However, PVDF membrane did not show the same strength as α-Al_2O_3 membrane.

To obtain high quality permeate, SDS is not recommended to added in POME for UF. α-Al_2O_3 membrane shown better performance than PVDF membrane in the aspects of lower stable TMP and better anti-fouling property. Although the number of cycles recommended for α-Al_2O_3 UF was merely 11 and frequent chemical cleaning would be needed, α-Al_2O_3 is a good choice for POME treatment due to its strong resistance to harsh chemicals.

6.2 EXPERIMENTAL SUGGESTIONS

Based on the experimental results and weaknesses, the suggestions for further research are given below:

1) In order to guarantee high rejection of oil in filtration process,before starting new cycles after chemical cleaning, the membrane is recommended to be flushed with POME for a short while to form oil layer for 99.5% rejection rate.

2) Small flux intervals such as 5 or 3 LMH are recommended to be applied to test α-Al_2O_3 membrane in 57-76LMH range and PVDF membrane in 38-57 LMH range to determine the critic fluxes of both membrane, respectively.

3) Repeat long term test of α-Al_2O_3 membrane until chemical cleaning fails or permeate quality encounters significant decrease to determine the life span of α-Al_2O_3 membrane

4) Membrane autopsy and SEM test of the fouling on PVDF and α-Al_2O_3 membranes are recommended to further analyze the morphology of fouling and determine the fouling mechanism.

5) Other types of surfactants are recommended to add in POME for the complete study of the interactions between surfactant and membrane surface.

6) Energy consumption at different operating conditions is recommended to be measured or calculated for further evaluation of industrial application of both membranes.

6.3 OUTLOOK

1) Due to the stable operational condition of α-Al_2O_3 and TMP, as well as great quality of permeate quality, both membranes could be directly implemented after simple pre-treatment such as sieving and gravity separation that remove solids and

oil slick, respectively. α-Al_2O_3 is highly recommended due to its higher oil and water recovery and lower TMP needed compared with PVDF membrane.

2) As POME is not toxic at all, the oil slicks in membrane concentrate can be collected and sent back to palm oil extraction line for oil production, and the remaining oil emulsion can be digested in bioreactor with smaller surface area, which enables less pollution discharge and extra benefit from POME treatment. Although membrane is still expensive, at least α-Al_2O_3 and PVDF membranes can promise good effluent quality that can be discharged or reused, avoiding serious pollution that conventional pond-digester system brings. Beside, the development of membrane technology is expected to reduce membrane cost in the near future.

A CHARACTERISTICS OF POME

A.1 PHYSICO-CHEMICAL CHARACTERISTICS OF RAW POME

Table A.1: The physicochemical characteristics of POME.

Parameter	Unit	Value	Reference
pH	-	3.9-5	[Habib et al., 1997; Fang et al., 2011; Chin et al., 2013]
DO(Dissolved Oxygen)	mg/L	2.57-4.69	[Ohimain et al., 2013]
EC(Electrical Conductivity)	μs /cm	137	[Okogbenin et al., 2014]
Total COD	mg COD/L	42900-88250	[Wood et al., 1979; Tabassum et al., 2015; Ohimain and Izah, 2017]
Soluble COD	mg COD/L	45000-88000	[Fang et al., 2011; Yoochatchaval et al., 2011]
BOD	mg/L	17000-65714	[Wood et al., 1979; Chin et al., 2013; Tabassum et al., 2015]
TS(Total Solids)	mg/L	30000-100000	[Borja et al., 1996; Chin et al., 2013; Tabassum et al., 2015]
VS (Volatile solids)	mg/L	24300-80000	[Borja et al., 1996]
VSS (Volatile suspended solids)	mg/L	8100-28500	[Borja et al., 1996]
SS (suspended solids)	mg/L	14100-50000	[Wood et al., 1979]
Alkalinity	mg/L	148-536	[Fang et al., 2011; Tabassum et al., 2015]
T-protein	mg/L	8830-21150	[Yoochatchaval et al., 2011]
T-sugar	mg/L	15320-26330	[Yoochatchaval et al., 2011]
Oil and Grease	mg/L	4000-15900	[Yoochatchaval et al., 2011]
Lipid	mg/L	8400	[Fang et al., 2011]
Ethanol	mmol/L	12.45	[Fang et al., 2011]
Butyric acid	mmol/L	0.18	[Fang et al., 2011]
Acetic acid	mmol/L	52.62	[Fang et al., 2011]
Propionic acid	mmol/L	0.78	[Fang et al., 2011]
Total VFA	mg/L	3300	[Fang et al., 2011]
TN(Total Nitrogen)	mg/L	500-900	[Wood et al., 1979; Borja et al., 1996; Chin et al., 2013]
TKN	mg/L	3200	[Fang et al., 2011]
SO_4	mg/L	60-66	[Borja et al., 1996; Awotoye et al., 2011]
NO_3	mg/L	262.26	[Awotoye et al., 2011]
k	mg/L	1281-1928	[Wood et al., 1979]
Mg	mg/L	254-344	[Wood et al., 1979]
Na	mg/L	225-332	[Awotoye et al., 2011; Okogbenin et al., 2014]
Ca	mg/L	252-605	[Wood et al., 1979; Awotoye et al., 2011; Okogbenin et al., 2014; Ohimain and Izah, 2017]
Al	mg/L	120	[Borja et al., 1996; Ohimain and Izah, 2017]
B	mg/L	0.9	[Borja et al., 1996; Ohimain and Izah, 2017]
N	mg/L	365-800	[Borja et al., 1996; Wood et al., 1979]
P	mg/L	17-165	[Wood et al., 1979; Awotoye et al., 2011; Okogbenin et al., 2014]
Cd	mg/L	0.01-0.03	[Wood et al., 1979; Ohimain et al., 2013]
Cu	mg/L	0.6-2.44	[Wood et al., 1979; Ohimain et al., 2013, 2012]
Fe	mg/L	6-205	[Wood et al., 1979; Borja et al., 1996; Ohimain et al., 2013]
Cr	mg/L	0.05-0.43	[Wood et al., 1979]
Zn	mg/L	1.2-6	[Wood et al., 1979; Borja et al., 1996]
Mo	mg/L	0.1	[Borja et al., 1996]
Mn	mg/L	2-34	[Wood et al., 1979; Awotoye et al., 2011]
Ni	mg/L	1.2	[Borja et al., 1996; Ohimain and Izah, 2017]
Si	mg/L	55	[Borja et al., 1996; Ohimain and Izah, 2017]
Ba	mg/L	0.3	[Borja et al., 1996; Ohimain and Izah, 2017]
Co	mg/L	0.01-0.06	[Borja et al., 1996; Wood et al., 1979]

Table A.2: The characteristics of fatty acids – pKa, composition, structural formula, surface tension and carbon oxygen ratio (C/O)

LCFA Type	Chemical Formula	Composition (v/v%)	pKa	Structural Formula	Surface Tension (mN/m)	C/O (mol/-mol)	Reference
Palmitic acid (16:0)	$C_6H_{32}O2$	22.45	4.95		28.2	8	[Lai et al., 1996; Mancini et al., 2015; Kim et al., 2019]
Oleic acid (18:1n-9)	$C_{18}H_{34}O2$	14.54	9.85	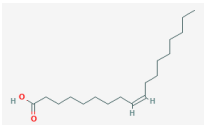	29.6	9	[Chumpitaz et al., 1999; Kanicky and Shah, 2002; Monde et al., 2009; Amin et al., 2010; Mancini et al., 2015]
Myristic acid (14:0)	$C_{14}H_{28}O2$	12.66	4.75		27.86	7	[Burdock and Carabin, 2007]
Stearic acid (18:0)	$C_{18}H_{36}O2$	10.41	10.15	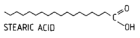	-	9	[Zock and Katan, 1992; Kanicky and Shah, 2002]
Linoleic acid (18:2n-6)	$C_{18}H_{32}O2$	9.53	4.77	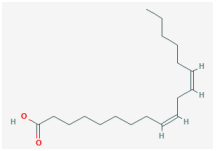	-	9	[Zock and Katan, 1992; Kanicky and Shah, 2002; Monde et al., 2009; Kim et al., 2019]
Linolenic acid (18:3n-3)	$C_{18}H_{30}O2$	4.72	8.28	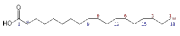	-	9	[Kanicky and Shah, 2002; Monde et al., 2009]
Capric acid (10:0)	$C_{10}H_{20}O2$	4.29	4.9		5.0	5	[Kim et al., 2019]
Arachidic acid (20:0)	$C_{20}H_{40}O2$	3.56	-		-	10	[Kim et al., 2019]
Lauric acid (12:0)	$C_{12}H_{24}O2$	3.22	5.3		26.6	6	[Kim et al., 2019]
Caprylic acid (8:0)	$C_8H_{16}O2$	2.37	4.89	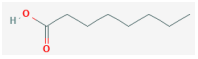	23.7	4	[Kim et al., 2019]
Pentadecanoic acid (15:0)	$C_{15}H_{30}O2$	2.21	4.78		-	7.5	[Kim et al., 2019; Drouin et al., 2010]
Eicosatrienoic acid (20:3n6)	$C_{20}H_{34}O2$	2.04	-	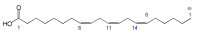	-	10	[Monde et al., 2009]
Heptadecanoic acid (17:0)	$C_{17}H_{34}O2$	1.39	-		-	8.5	[Kim et al., 2019]
10-Heptadecanoic acid (17:1)	$C_{17}H_{32}O2$	1.12	-	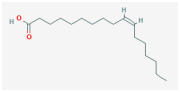	-	8.5	[Kim et al., 2019]
Eicosatetraenoic acid (20:4n6)	$C_{20}H_{32}O2$	1.12	-	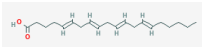	-	10	[Kim et al., 2019]
Eicosapentaenoic acid (20:5n3)	$C_{20}H_{30}O2$	0.36	-	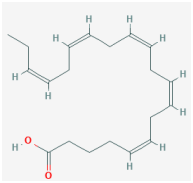	-	9	[Kim et al., 2019; Monde et al., 2009]

Table A.3: Types of dominant LCFAs in POME.

LCFA Type	Unit	Value	Reference
Linoleic acid (C18:2)	mg/L	400	[Yoochatchaval et al., 2011]
Oleic acid (C18:1)	mg/L	2500	[Yoochatchaval et al., 2011]
Stearic acid (C18:0)	mg/L	400	[Yoochatchaval et al., 2011]
Palmitic acid (C16:0)	mg/L	2880	[Yoochatchaval et al., 2011]
Myristic acid (C14:0)	mg/L	20	[Yoochatchaval et al., 2011]

A.2 GUIDELINES FOR POME TREATMENT AND WATER REUSE

Table A.4: Effluent discharge standards for crude palm oil mills(Environmental Quality Act 1974, 2005) [Rupani et al., 2010]

Parameter	Unit	Discharge Standard	Remarks
BOD;30 day 30°C	mg/L	100	-
COD	mg/L	*	-
Total Solids	mg/L	*	-
Suspended Solids	mg/L	400	-
Oil and grease	mg/L	50	-
Ammoniacal Nitrogen	mg/L	150	Value of filtered sample
Total Nitrogen	mg/L	200	Value of filtered sample
pH	-	5-9	-
Temperature	°C	45	-

Table A.5: Guidelines for wastewater reuse provided by WHO [Saleem et al., 2011; Azmi et al., 2013] and discharge in Malaysia [Ahmad et al., 2003].

Parameter	Unit	Discharge Limit	Reuse Limit
pH	-	5-7	6-9
Turbidity	NTU	-	-
Oil and grease	mg/L	50	8.0
BOD	mg/L	100	200
COD	mg/L	-	500
TDS	mg/L	-	1500
TSS	mg/L	400	150
Total Nitrogen	mg/L	150	70

A.3 PSD AND ZETA POTENTIAL OF POME AND PH EFFECT ON OIL HYDROLYSIS

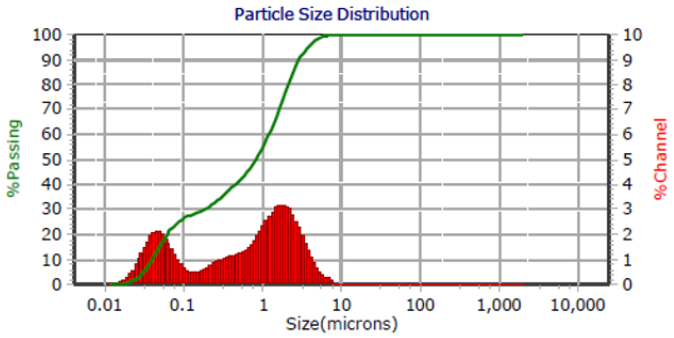

Figure A.1: Oil droplet size distribution of POME-SDS (Peak summary: [Diameter-v/v%]:1.329 μm -73.4%; 0.046 μm -26.6%).

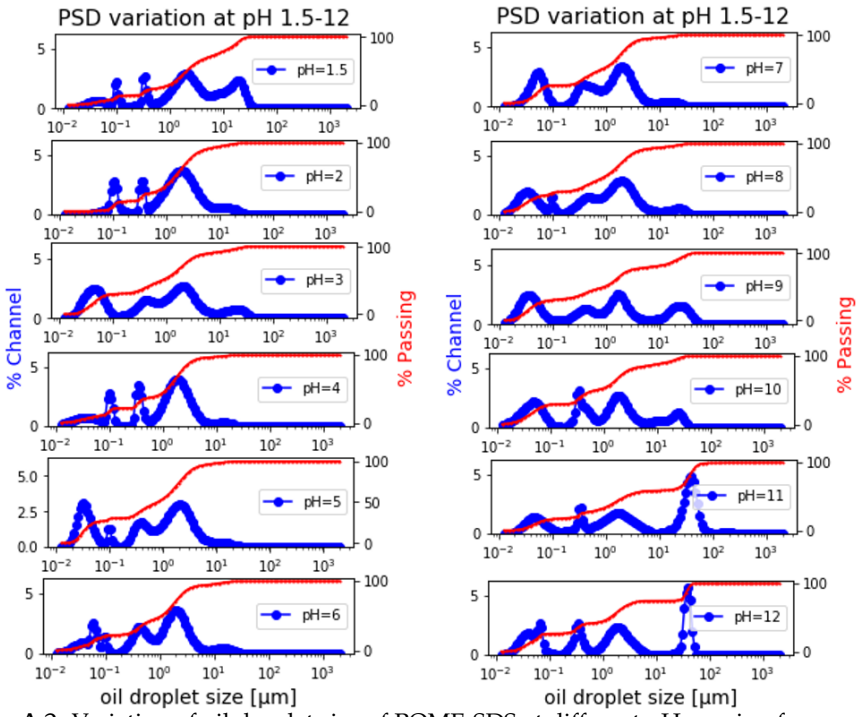

Figure A.2: Variation of oil droplet size of POME-SDS at different pH ranging from 1.5 to 12.

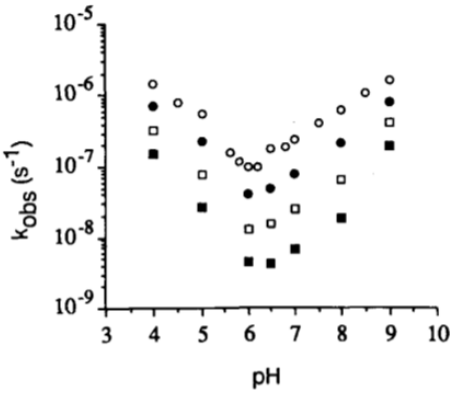

Figure A.3: The effect of pH on the hydrolysis of PHEPC (C = 0.05M). Each point represents the mean of the two separate measurement. ○70, ·60□50, ■40°C.[GRIT et al., 1993]

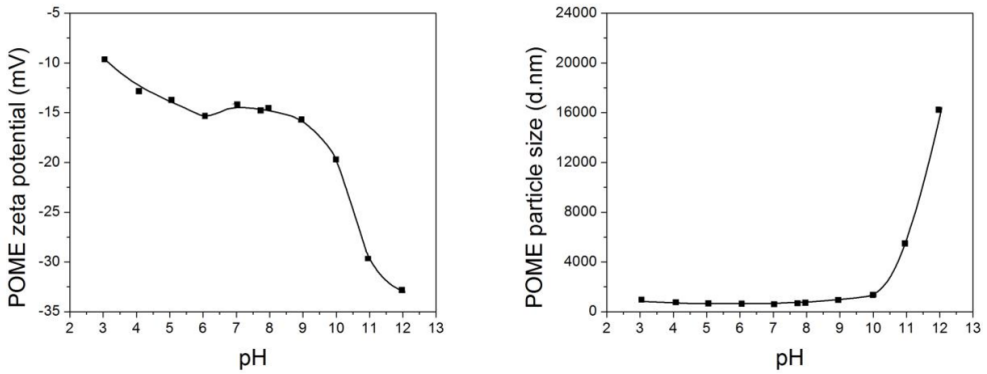

Figure A.4: The variation of zeta potential (left) and particle size (right) of real POME (without surfactant addition) at different pH ranging from 3 to 11.Azmi and Omar

B RATIOS OF COD TO CONCENTRATION

B.1 THE RATIO OF COD TO OIL CONCENTRATION

To convert COD value to oil concentration in POME, the theoretical ratio of COD to palm oil weight is calculated. Like all lipids, 1 mole palm oil is composed of 1 mole glycerol and 3 moles LCFA. Firstly, five quantitively dominant LCFAs in Table I-2 were selected as the representative compositions in POME, and tabulated in Table II-1. Secondly, the average ratio of COD to LCFA mass was calculated by Eq.II-1 and the average molecular weight of LCFAs was calculated by Eq.II-1, based on the molecular weight, ratio and percentage of each LCFA in Table II-1. Lastly, the ratio of COD to oil weight was determined by Eq. II-3, based on the aforementioned calculated values and 3:1 LCFA to glycerol ratio.

Table B.1: The ratio of COD to weight of LVFA and glycerol

Parameter	Unit	Glycerol	Palmitic Acid	Oleic Acid	Myristic Acid	Stearic Acid	Linoleic Acid
Percentage	%	-	22.45	14.54	12.66	10.41	9.53
Molecular Weight	g/mol	92	256	282	228	284	280
COD	g COD/mol	112	736	816	640	832	800
COD/Mass	g COD/g substance	1.217	2.875	2.894	2.807	2.930	2.857

$$MW_{LCFA_{average}} = \frac{\sum MW_{LCFA_i} \times Percentage_{LCFA_i}}{\sum Percentage_{LCFA_i}} = 263.814 g/mol \tag{B.1}$$

$$Ratio_{\frac{COD}{LCFA_{average}}} = \frac{\sum Ratio_{LCFA_i} \times Percentage_{LCFA_i}}{\sum Percentage_{LCFA_i}} = 2.872 \frac{gCOD}{gLCFA} \tag{B.2}$$

$$Ratio_{\frac{COD}{oil_{average}}} = \frac{Ratio_{\frac{COD}{glycerol}} \times 1 + Ratio_{\frac{COD}{LCFA_{average}}} \times M_{LCFA_{average}} \times 3}{M_{glycerol} \times 1 + M_{LCFA_{average}} \times 3} = 2.7 \frac{gCOD}{gOil} \tag{B.3}$$

B.2 THE RATIO OF COD TO SDS CONCENTRATION

Based on the prepared SDS solutions with certain concentrations and the corresponding COD values measured by Hach kits, the relation was plotted in Figure B1 below. The two parameters shows liner relation, which can be explained by Equation B1 below as well, with R2 value of 0.9985.

$$_{SDS} = 2.0199 \times Conc._{SDS} + 6.4 \tag{B.4}$$

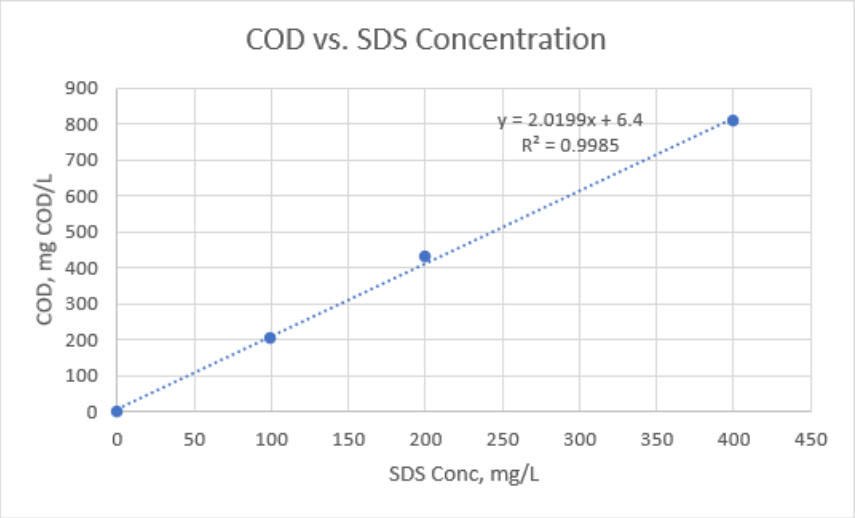

B.3 THE RELATION BETWEEN PALM OIL CONCENTRATION AND PEAK HEIGHT IN ABSORBANCE SPECTROSCOPY

Table B.2: The relation between palm oil concentration and peak height in absorbance spectroscopy

COD_{POME}	10983	2600.7	1214.7	627.7	232.3	119.0	50.8	30.7	20.2	15.6
$Wavelength_{peak}$	292.5	296.5	296.0	296.0	294.0	293.5	293.5	293.5	293.5	293.5
Abs_{peak}	3.7	2.3	1.7	1.1	0.5	0.3	0.2	0.1	0	0
SD_COD	279.0	24.9	7.6	4.6	1.2	0.8	1.1	1.6	1.3	0.8

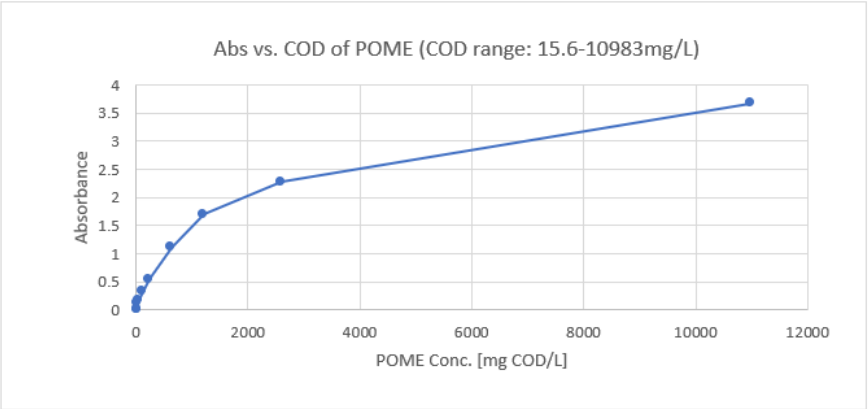

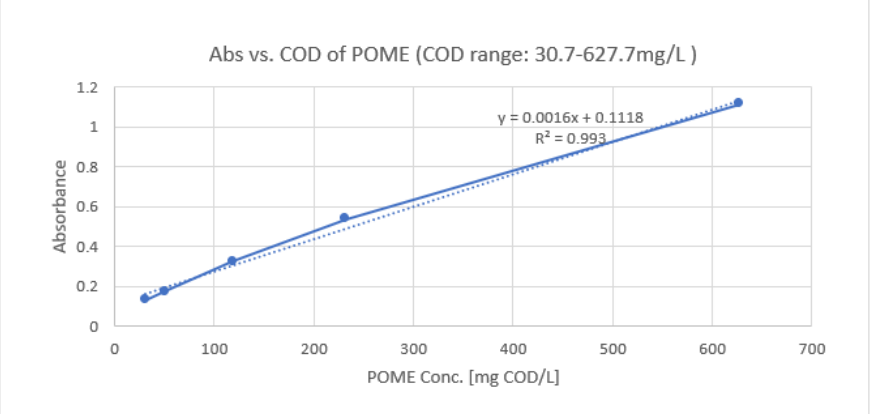

C ADDITIONAL UF INFORMATION

C.1 SETUP SETTING IN PERMEABILITY TEST

Table C.1: Operation conditions of valves and pumps in the phases of permeability test.("+": open/turned on, "-": closed/turned off)

No.	Phase	Valve 1	Valve 2	Valve 3	Valve 4	Valve 5	Feed Pump	Circulation Pump
1	Forward Flush	-	+	+	+	-	-	+
2	Filtration	-	+	-	-	+	+	+

C.2 α-AL_2O_3 MEMBRANE UF OF POME AT LOW CFV AND PERMEATE FLUX

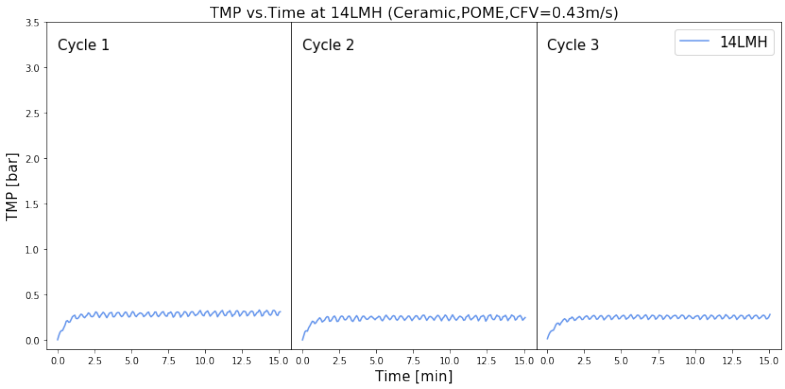

Figure C.1: Three cycles of POME α-Al_2O_3 membrane filtration at 14LMH (CFV=0.43m/s)

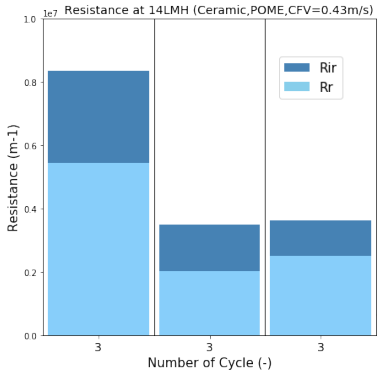

Figure C.2: Resistance of α-Al_2O_3 membrane treating POME at 14LMH (CFV=0.43m/s)

D EFFECT OF SDS AT DIFFERENT PH

D.1 EFFECT OF SDS ON PVDF MEMBRANE PERFORMANCE AT DIFFERENT PH

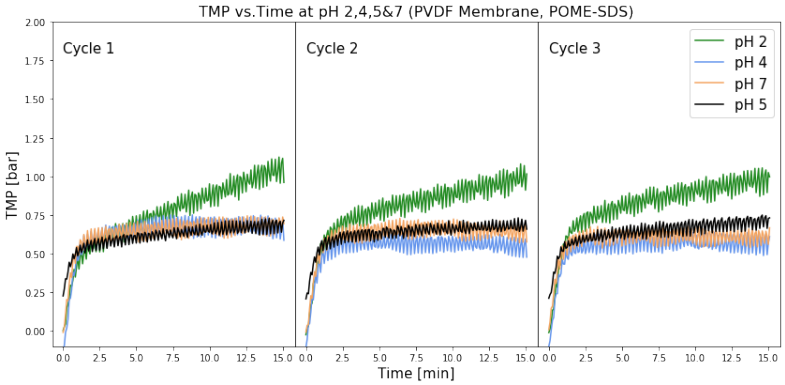

Figure D.1: Three cycles of POME-SDS PVDF membrane filtration at pH 2,4,5 and 7 (CFV = 0.43m/s,Permeate Flux = 28LMH).

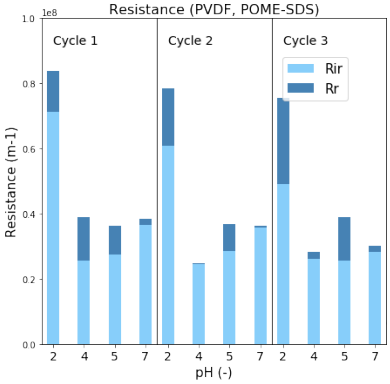

Figure D.2: Rr and Rir variation of PVDF membrane when treating POME with SDS at pH 2, 4, 5 & 7 (CFV = 0.78m/s, Permeate Flux =38 LMH).

In comparison of Figure 5.9 and D.1 for PVDF membrane, the effect of pH on UF of POME-SDS shown the same trend as of POME without SDS except for PVDF filtration at pH 4.

This section studied the effect of pH on POME-SDS UF and compared it with POME UF at the same conditions. Observing TMP variation of Figure 5.9 and D.1, except for pH 4, the addition of SDS did not change the distinction of TMP variation below and above IEP_{PVDF}. Like negatively charged oil droplets in POME, SDS molecules and oil droplets with SDS surrounded (both negatively charged) in POME-SDS were rejected by membrane above IEP_{PVDF} and adsorbed below that, via electrostatic repulsion and attraction, respectively.

However, the addition of SDS could magnify the effect of pH on UF performance and increased membrane resistance owing to the extra fouling source. When pH

decreased from 5 to 2, membrane resistance (Rir+Rr) of POME-SDS filtration increased from 3.38×10^7 to 7.54×10^7 m^{-1} (1.23 times increment) in the third cycle, while without SDS addition, it increased from 2.8×10^7 to 5.0×10^7 m^{-1} (0.78 times increment).

With regards to pH 4, SDS addition significantly improved membrane's anti-fouling property - stabilizing TMP and avoiding sharp TMP increase. The increase of negative charge on oil droplets caused by SDS addition enhanced electrostatic repulsion between membrane and oil droplets. Zeta potential of raw POME (-19 -15mV [Lek et al., 2018; Zahrim et al., 2014]) and that of POME-SDS (-50mV, tested in this project) were the evidence for charge variation of oil droplets.

D.2 EFFECT OF SDS ON α-AL_2O_3 MEMBRANE PERFORMANCE AT DIFFERENT PH

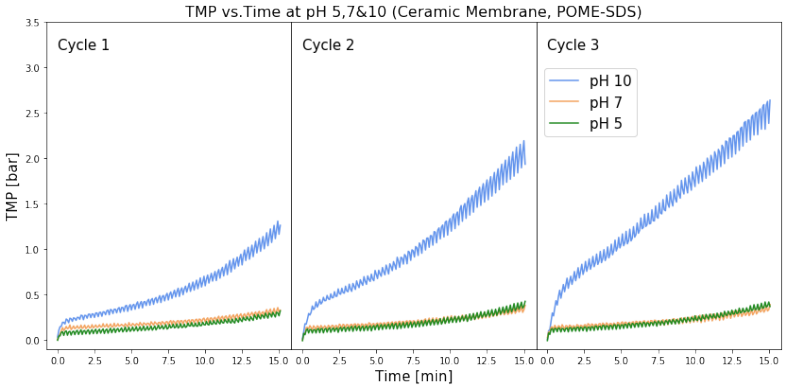

Figure D.3: Three cycles of POME-SDS α-Al_2O_3 membrane filtration at pH 5, 7and 10 (CFV = 0.43m/s,Permeate Flux = 28LMH).

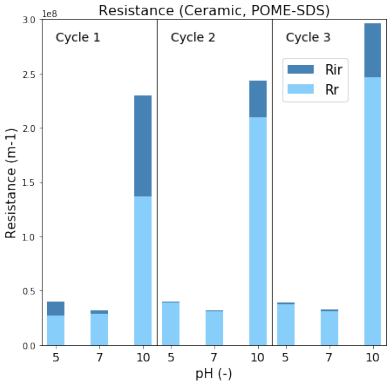

Figure D.4: Rr and Rir variation of α-Al_2O_3 membrane when treating POME with SDS at pH 5, 7 and 10 (CFV = 0.43m/s, Permeate Flux = 28 LMH).

In comparison of Figure 5.9 and D.1 for PVDF membrane, as well as of Figure, 5.19 and D.4 for α-Al_2O_3 membrane, the effect of pH on UF of POME-SDS shown the same trend as of POME without SDS except for PVDF filtration at pH 4. Thus SDS addition didn't change pH effect on POME filtration performance. The reason of the similarity of α-Al_2O_3 membrane was, the 2-layer SDS and oil layer were formed at the same pH (pH 5 and 7) for α-Al_2O_3 membrane, respectively, transforming electrostatic attraction to repulsion and increasing anti-fouling capability. While at pH 10, with SDS getting concentrated in the feed side in UF process and the continuous flushing of feed, one layer of SDS could be loosely formed close to mem-

brane with hydrophobic tail towards feed solution as Figure **??**, which weakened membrane hydrophilicity thus water permeability was reduced and more fouling formed. In this process the one layer SDS not only didn't modify α-Al_2O_3 membrane as the neatly arranged doulbe layers, but negatively affect the membrane property. Resistance variation along pH range also shown the same conclusion, that was, the resistance of α-Al_2O_3 membrane increased more dramatically with the addition of SDS. As pH increased from 5 to 10, membrane resistance (Rir+Rr) of POME-SDS filtration increased from 0.39×10^8 to 2.96^8 m^{-1} (6.6 times increment) in the third cycle, while for POME filtration, it increased from 0.297×10^7 to 1.97×10^7 m^{-1} (5.6 times increment).

BIBLIOGRAPHY

Sareh Rezaei Hosein Abadi, Mohammad Reza Sebzari, Mahmood Hemati, Fatemeh Rekabdar, and Toraj Mohammadi. Ceramic membrane performance in microfiltration of oily wastewater. *Desalination*, 265(1-3):222–228, 2011.

Abdul Latif Ahmad, Suzylawati Ismail, and Subhash Bhatia. Water recycling from palm oil mill effluent (pome) using membrane technology. *Desalination*, 157 (1-3):87–95, 2003.

Anwar Ahmad and Roomana Ghufran. Review on industrial wastewater energy sources and carbon emission reduction: towards a clean production. *International Journal of Sustainable Engineering*, 12(1):47–57, 2019.

Tausif Ahmad, Chandan Guria, and Ajay Mandal. A review of oily wastewater treatment using ultrafiltration membrane: A parametric study to enhance the membrane performance. *Journal of Water Process Engineering*, 36:101289, 2020.

Yunus Ahmed, Zahira Yaakob, Parul Akhtar, and Kamaruzzaman Sopian. Production of biogas and performance evaluation of existing treatment processes in palm oil mill effluent (pome). *Renewable and Sustainable Energy Reviews*, 42: 1260–1278, 2015.

Indok Nurul Hasyimah Mohd Amin, Abdul Wahab Mohammad, Mastura Markom, and Leo Choe Peng. Effects of palm oil-based fatty acids on fouling of ultrafiltration membranes during the clarification of glycerin-rich solution. *Journal of food engineering*, 101(3):264–272, 2010.

INHM Amin and AW Mohammad. Verification of a combined fouling model to predict flux decline during ultrafiltration of organic solutes. *Journal of Applied Membrane Science & Technology*, 22(2), 2018.

Ayse Asatekin, Seoktae Kang, Menachem Elimelech, and Anne M Mayes. Antifouling ultrafiltration membranes containing polyacrylonitrile-graft-poly (ethylene oxide) comb copolymer additives. *Journal of Membrane Science*, 298(1-2): 136–146, 2007.

OO Awotoye, AC Dada, GAO Arawomo, et al. Impact of palm oil processing effluent discharge on the quality of receiving soil and river in south western nigeria. *Journal of Applied Sciences Research*, 7(2):111–118, 2011.

Luqman Hakim Mohd Azmi and Fatehah Mohd Omar. Characterization and behaviour of palm oil mill effluent and polyaluminium chloride: Influence of ph.

Nazatul Shima Azmi, Khairul Faezah Md Yunos, Azhari Samsu Baharuddin, and Zanariah Md Dom. The effect of operating parameters on ultrafiltration and reverse osmosis of palm oil mill effluent for reclamation and reuse of water. *BioResources*, 8(1):76–87, 2013.

Yolaine Bessiere, Bruce Jefferson, Emma Goslan, and Patrice Bacchin. Effect of hydrophilic/hydrophobic fractions of natural organic matter on irreversible fouling of membranes. *Desalination*, 249(1):182–187, 2009.

Rafael Borja, Charles J Banks, and Enrique Sánchez. Anaerobic treatment of palm oil mill effluent in a two-stage up-flow anaerobic sludge blanket (uasb) system.

Journal of Biotechnology, 45(2):125–135, 1996.

J Brinck, A-S Jönsson, Bengt Jönsson, and J Lindau. Influence of ph on the adsorptive fouling of ultrafiltration membranes by fatty acid. *Journal of Membrane Science*, 164(1-2):187–194, 2000.

George A Burdock and Ioana G Carabin. Safety assessment of myristic acid as a food ingredient. *Food and chemical toxicology*, 45(4):517–529, 2007.

Henric Byhlin and A-S Jönsson. Influence of adsorption and concentration polarisation on membrane performance during ultrafiltration of a non-ionic surfactant. *Desalination*, 151(1):21–31, 2003.

Christel Causserand, Sandrine Rouaix, Ahmad Akbari, and Pierre Aimar. Improvement of a method for the characterization of ultrafiltration membranes by measurements of tracers retention. *Journal of Membrane Science*, 238(1-2):177–190, 2004.

B Chakrabarty, AK Ghoshal, and MK Purkait. Ultrafiltration of stable oil-in-water emulsion by polysulfone membrane. *Journal of Membrane Science*, 325(1):427–437, 2008.

Mingliang Chen, Ran Shang, Paolo M Sberna, Mieke WJ Luiten-Olieman, Luuk C Rietveld, and Sebastiaan GJ Heijman. Highly permeable silicon carbide-alumina ultrafiltration membranes for oil-in-water filtration produced with low-pressure chemical vapor deposition. *Separation and Purification Technology*, 253:117496, 2020.

May Ji Chin, Phaik Eong Poh, Beng Ti Tey, Eng Seng Chan, and Kit Ling Chin. Biogas from palm oil mill effluent (pome): Opportunities and challenges from malaysia's perspective. *Renewable and Sustainable Energy Reviews*, 26:717–726, 2013.

Lucy DA Chumpitaz, Lilian F Coutinho, and Antonio JA Meirelles. Surface tension of fatty acids and triglycerides. *Journal of the American Oil Chemists' Society*, 76 (3):379–382, 1999.

Tibor Cserháti, Esther Forgács, and Gyula Oros. Biological activity and environmental impact of anionic surfactants. *Environment international*, 28(5):337–348, 2002.

Laura De Angelis and María Marta Fidalgo de Cortalezzi. Ceramic membrane filtration of organic compounds: Effect of concentration, ph, and mixtures interactions on fouling. *Separation and Purification Technology*, 118:762–775, 2013.

Wiebe M de Vos and Saskia Lindhoud. Overcharging and charge inversion: Finding the correct explanation (s). *Advances in colloid and interface science*, 274:102040, 2019.

Sylvain Drouin, Mohammed Boussafir, Jean-Louis Robert, Patrick Albéric, and Aude Durand. Carboxylic acid sorption on synthetic clays in sea water: in vitro experiments and implications for organo-clay behaviour under marine conditions. *Organic geochemistry*, 41(2):192–199, 2010.

G Duplatre, MF Ferreira Marques, and M da Graça Miguel. Size of sodium dodecyl sulfate micelles in aqueous solutions as studied by positron annihilation lifetime spectroscopy. *The Journal of physical chemistry*, 100(41):16608–16612, 1996.

Cheng Fang, O Sompong, Kanokwan Boe, Irini Angelidaki, et al. Comparison of uasb and egsb reactors performance, for treatment of raw and deoiled palm oil mill effluent (pome). *Journal of Hazardous Materials*, 189(1-2):229–234, 2011.

Eva Fernández, José Manuel Benito, Carmen Pazos, and José Coca. Ceramic membrane ultrafiltration of anionic and nonionic surfactant solutions. *Journal of Membrane Science*, 246(1):1–6, 2005.

PS Goh and AF Ismail. A review on inorganic membranes for desalination and wastewater treatment. *Desalination*, 434:60–80, 2018.

MUSTAFA GRIT, NICOLAAS J ZUIDAM, WILLY JM UNDERBERG, and DAAN JA CROMMELIN. Hydrolysis of partially saturated egg phosphatidylcholine in aqueous liposome dispersions and the effect of cholesterol incorporation on hydrolysis kinetics. *Journal of pharmacy and pharmacology*, 45(6):490–495, 1993.

MAB Habib, FM Yusoff, SM Phang, KJ Ang, and S Mohamed. Nutritional values of chironomid larvae grown in palm oil mill effluent and algal culture. *Aquaculture*, 158(1-2):95–105, 1997.

N Awanis Hashim, Fu Liu, and K Li. A simplified method for preparation of hydrophilic pvdf membranes from an amphiphilic graft copolymer. *Journal of Membrane Science*, 345(1-2):134–141, 2009.

Charles A Haynes and Willem Norde. Globular proteins at solid/liquid interfaces. *Colloids and Surfaces B: Biointerfaces*, 2(6):517–566, 1994.

Zhengwang He, Daniel J Miller, Sirirat Kasemset, Lu Wang, Donald R Paul, and Benny D Freeman. Fouling propensity of a poly (vinylidene fluoride) microfiltration membrane to several model oil/water emulsions. *Journal of Membrane Science*, 514:659–670, 2016.

Zhengwang He, Sirirat Kasemset, Alon Y Kirschner, Yu-Heng Cheng, Donald R Paul, and Benny D Freeman. The effects of salt concentration and foulant surface charge on hydrocarbon fouling of a poly (vinylidene fluoride) microfiltration membrane. *Water research*, 117:230–241, 2017.

HP Hsieh. *Inorganic membranes for separation and reaction*. Elsevier, 1996.

FL Hua, Yiu Fai Tsang, YJ Wang, SY Chan, H Chua, and SN Sin. Performance study of ceramic microfiltration membrane for oily wastewater treatment. *Chemical Engineering Journal*, 128(2-3):169–175, 2007.

Xin Huang, Weiping Wang, Yaodong Liu, Hui Wang, Zhibing Zhang, Wenling Fan, and Lei Li. Treatment of oily waste water by pvp grafted pvdf ultrafiltration membranes. *Chemical Engineering Journal*, 273:421–429, 2015.

M Amirul Islam, Abu Yousuf, Ahasanul Karim, Domenico Pirozzi, Maksudur Rahman Khan, and Zularisam Ab Wahid. Bioremediation of palm oil mill effluent and lipid production by lipomyces starkeyi: a combined approach. *Journal of Cleaner Production*, 172:1779–1787, 2018.

Hesam Kamyab, Ferenc Friedler, Jiri J Klemes, Shreeshivadasan Chelliapan, and Shahabaldin Rezania. Bioenergy production and nutrients removal by green microalgae with cultivation from agro-wastewater palm oil mill effluent (pome)-a review. *Chemical Engineering Transactions*, 70:2197–2202, 2018.

James R Kanicky and Dinesh O Shah. Effect of degree, type, and position of unsaturation on the pka of long-chain fatty acids. *Journal of colloid and interface science*, 256(1):201–207, 2002.

Sunghwan Kim, Jie Chen, Tiejun Cheng, Asta Gindulyte, Jia He, Siqian He, Qingliang Li, Benjamin A Shoemaker, Paul A Thiessen, Bo Yu, et al. Pubchem 2019 update: improved access to chemical data. *Nucleic acids research*, 47(D1): D1102–D1109, 2019.

Yogesh Kumar, KM Popat, H Brahmbhatt, B Ganguly, and A Bhattacharya. Pentachlorophenol removal from water using surfactant-enhanced filtration through low-pressure thin film composite membranes. *Journal of hazardous materials*, 154(1-3):426–431, 2008.

June WS Lai, Linda J Pinto, Leah I Bendell-Young, Margo M Moore, and Eberhard Kiehlmann. Factors that affect the degradation of naphthenic acids in oil sands wastewater by indigenous microbial communities. *Environmental Toxicology and Chemistry: An International Journal*, 15(9):1482–1491, 1996.

Oi-Ming Lai, Chin-Ping Tan, and Casimir C Akoh. *Palm oil: production, processing, characterization, and uses*. Elsevier, 2015.

Jieun Lee, Sanghyun Jeong, Yun Ye, Vicki Chen, Saravanamuthu Vigneswaran, TorOve Leiknes, and Zongwen Liu. Protein fouling in carbon nanotubes enhanced ultrafiltration membrane: fouling mechanism as a function of ph and ionic strength. *Separation and Purification Technology*, 176:323–334, 2017.

Brian Lee Choong Lek, Angela Paul Peter, Kevin Hwang Qi Chong, Pavithran Ragu, Vasanthi Sethu, Anurita Selvarajoo, and Senthil Kumar Arumugasamy. Treatment of palm oil mill effluent (pome) using chickpea (cicer arietinum) as a natural coagulant and flocculant: Evaluation, process optimization and characterization of chickpea powder. *Journal of environmental chemical engineering*, 6(5): 6243–6255, 2018.

Qilin Li and Menachem Elimelech. Synergistic effects in combined fouling of a loose nanofiltration membrane by colloidal materials and natural organic matter. *Journal of Membrane Science*, 278(1-2):72–82, 2006.

Yi-Min Lin and Gregory C Rutledge. Separation of oil-in-water emulsions stabilized by different types of surfactants using electrospun fiber membranes. *Journal of membrane science*, 563:247–258, 2018.

Alberto Lobo, Ángel Cambiella, José Manuel Benito, Carmen Pazos, and José Coca. Ultrafiltration of oil-in-water emulsions with ceramic membranes: Influence of ph and crossflow velocity. *Journal of Membrane Science*, 278(1-2):328–334, 2006.

J Lyklema. Adsorption of ionic surfactants on clay minerals and new insights in hydrophobic interactions. In *Surfactants and Colloids in the Environment*, pages 91–97. Springer, 1994.

Sayed Siavash Madaeni, Hossein Ahmadi Monfared, Vahid Vatanpour, Ahmad Arabi Shamsabadi, Ehsan Salehi, Parisa Daraei, Saeed Laki, and Sayed Mehdi Khatami. Coke removal from petrochemical oily wastewater using γ-al203 based ceramic microfiltration membrane. *Desalination*, 293:87–93, 2012.

Annamaria Mancini, Esther Imperlini, Ersilia Nigro, Concetta Montagnese, Aurora Daniele, Stefania Orrù, and Pasqualina Buono. Biological and nutritional properties of palm oil and palmitic acid: effects on health. *Molecules*, 20(9):17339–17361, 2015.

R Margesin and F Schinner. Biodegradation of diesel oil by cold-adapted microorganisms in presence of sodium dodecyl sulfate. *Chemosphere*, 38(15):3463–3472, 1999.

María Matos, Gemma Gutiérrez, Alberto Lobo, José Coca, Carmen Pazos, and José M Benito. Surfactant effect on the ultrafiltration of oil-in-water emulsions using ceramic membranes. *Journal of Membrane Science*, 520:749–759, 2016.

Sandra C Medina, Andreia SF Farinha, Abdul-Hamid Emwas, Assiyeh Tabatabai, and TorOve Leiknes. A fundamental study of adsorption kinetics of surfactants onto metal oxides using quartz crystal microbalance with dissipation (qcm-d). *Colloids and Surfaces A: Physicochemical and Engineering Aspects*, 586:124237, 2020.

Amit Mehta and Andrew L Zydney. Permeability and selectivity analysis for ultrafiltration membranes. *Journal of membrane science*, 249(1-2):245–249, 2005.

M Mellyanawaty, FMA Chusna, H Sudibyo, N Nurjanah, and W Budhijanto. Influence of nutrient impregnated into zeolite addition on anaerobic digestion of palm oil mill effluent (pome). *MS&E*, 316(1):012069, 2018.

P Monash and G Pugazhenthi. Effect of tio2 addition on the fabrication of ceramic membrane supports: A study on the separation of oil droplets and bovine serum albumin (bsa) from its solution. *Desalination*, 279(1-3):104–114, 2011.

Absalome A Monde, Françoise Michel, Marie-Annette Carbonneau, Georges Tiahou, Marie-Hélène Vernet, Sabrina Eymard-Duvernay, Stephanie Badiou, Benjamin Adon, Eugène Konan, Daniel Sess, et al. Comparative study of fatty acid composition, vitamin e and carotenoid contents of palm oils from four varieties of oil palm from côte d'ivoire. *Journal of the Science of Food and Agriculture*, 89(15): 2535–2540, 2009.

N Nabi, P Aimar, and M Meireles. Ultrafiltration of an olive oil emulsion stabilized by an anionic surfactant. *Journal of Membrane Science*, 166(2):177–188, 2000.

JC Nnaji, JA Okoye, and SK Omotugba. Soil quality in the vicinity of palm oil mills in umuahia, nigeria. *International Research Journal of Chemistry and Chemical Sciences*, 3(1):029–032, 2016.

A Norhidayu, M Nur-Syazwani, R Radzil, I Amin, and N Balu. The production of crude palm oil in malaysia. *International Journal of Economics and Management*, 11(S3):591–606, 2017.

NA Ochoa, M Masuelli, and J Marchese. Effect of hydrophilicity on fouling of an emulsified oil wastewater with pvdf/pmma membranes. *Journal of Membrane Science*, 226(1-2):203–211, 2003.

Elijah I Ohimain, Enetimi I Seiyaboh, Sylvester C Izah, V Oghenegueke, and T Perewarebo. Some selected physico-chemical and heavy metal properties of palm oil mill effluents. *Greener Journal of Physical Sciences*, 2(4):131–137, 2012.

Elijah I Ohimain, Sylvester C Izah, and Nimi Jenakumo. Physicochemical and microbial screening of palm oil mill effluents for amylase production. *Greener Journal of Biological Sciences*, 3(8):307–318, 2013.

Elijah Ige Ohimain and Sylvester Chibueze Izah. A review of biogas production from palm oil mill effluents using different configurations of bioreactors. *Renewable and Sustainable Energy Reviews*, 70:242–253, 2017.

USDA Oilseeds. World markets and trade (february 2019 issue). *Office of Global Analysis: Foreign Agriculture Service: Washington DC, USA*, 2019.

OB Okogbenin, GE Anisiobi, EA Okogbenin, T Okunwaye, and A Ojieabu. Microbiological assessment and physiochemical parameters of palm oil mill effluent collected in a local mill in ovia north east area of edo state, nigeria. *Herald Journal of Microbiology and Biotechnology*, 1(1):001–009, 2014.

W Senyo Opong and Andrew L Zydney. Diffusive and convective protein transport through asymmetric membranes. *AIChE Journal*, 37(10):1497–1510, 1991.

Mahesh Padaki, R Surya Murali, Ms S Abdullah, Nurasyikin Misdan, A Moslehyani, MA Kassim, Nidal Hilal, and AF Ismail. Membrane technology enhancement in oil–water separation. a review. *Desalination*, 357:197–207, 2015.

Parveen Fatemeh Rupani, Rajeev Pratap Singh, M Hakimi Ibrahim, and Norizan Esa. Review of current palm oil mill effluent (pome) treatment methods: vermicomposting as a sustainable practice. *World Applied Sciences Journal*, 11(1): 70–81, 2010.

Muhammad Saleem, Alaadin A Bukhari, and Muhammad Noman Akram. Electrocoagulation for the treatment of wastewater for reuse in irrigation and plantation. *Journal of Basic & Applied Sciences*, 7(1), 2011.

Victoria A Shcherbakova, Kestutis S Laurinavichius, and Vasily K Akimenko. Toxic effect of surfactants and probable products of their biodegradation on methanogenesis in an anaerobic microbial community. *Chemosphere*, 39(11):1861–1870, 1999.

Salma Tabassum, Yejian Zhang, and Zhenjia Zhang. An integrated method for palm oil mill effluent (pome) treatment for achieving zero liquid discharge–a pilot study. *Journal of Cleaner Production*, 95:148–155, 2015.

Philippe Tounissou, Marc Hebrant, and C Tondre. On the behavior of micellar solutions in tangential ultrafiltration using mineral membranes. *Journal of colloid and interface science*, 183(2):491–497, 1996.

Emily N Tummons, Volodymyr V Tarabara, Jia Wei Chew, and Anthony G Fane. Behavior of oil droplets at the membrane surface during crossflow microfiltration of oil–water emulsions. *Journal of Membrane Science*, 500:211–224, 2016.

Mohammed Maikudi Usman, Arezoo Dadrasnia, Kang Tzin Lim, Ahmad Fahim Mahmud, and Salmah Ismail. Application of biosurfactants in environmental biotechnology; remediation of oil and heavy metal. *AIMS Bioengineering*, 3(3): 289–304, 2016.

Arne RD Verliefde, ER Cornelissen, SGJ Heijman, JQJC Verberk, GL Amy, B Van der Bruggen, and JC Van Dijk. The role of electrostatic interactions on the rejection of organic solutes in aqueous solutions with nanofiltration. *Journal of Membrane Science*, 322(1):52–66, 2008.

BJ Wood, KR Pillai, and JA Rajaratnam. Palm oil mill effluent disposal on land. *Agricultural Wastes*, 1(2):103–127, 1979.

Jeffrey Chi-Sheng Wu and En-Hsien Lee. Ultrafiltration of soybean oil/hexane extract by porous ceramic membranes. *Journal of Membrane Science*, 154(2):251–259, 1999.

Jiajian Xing, Heng Liang, Chong Joon Chuah, Yueping Bao, Xinsheng Luo, Tianyu Wang, Jinlong Wang, Guibai Li, and Shane A Snyder. Insight into fe (ii)/uv/chlorine pretreatment for reducing ultrafiltration (uf) membrane fouling: Effects of different natural organic fractions and comparison with coagulation. *Water research*, 167:115112, 2019.

W Yoochatchaval, S Kumakura, D Tanikawa, T Yamaguchi, MFM Yunus, SS Chen, K Kubota, H Harada, and K Syutsubo. Anaerobic degradation of palm oil mill effluent (pome). *Water Science and Technology*, 64(10):2001–2008, 2011.

Haisu Yu, Lizhong Zhu, and Wenjun Zhou. Enhanced desorption and biodegradation of phenanthrene in soil–water systems with the presence of anionic–nonionic mixed surfactants. *Journal of Hazardous Materials*, 142(1-2):354–361, 2007.

Li Yu, Mei Han, and Fang He. A review of treating oily wastewater. *Arabian journal of chemistry*, 10:S1913–S1922, 2017.

AY Zahrim, A Nasimah, and Nidal Hilal. Pollutants analysis during conventional palm oil mill effluent (pome) ponding system and decolourisation of anaerobically treated pome via calcium lactate-polyacrylamide. *Journal of Water Process Engineering*, 4:159–165, 2014.

Jia-ai Allen Zhang and John Pawelchak. Effect of ph, ionic strength and oxygen burden on the chemical stability of epc/cholesterol liposomes under accelerated conditions: Part 1: Lipid hydrolysis. *European journal of pharmaceutics and biopharmaceutics*, 50(3):357–364, 2000.

Zhaoxiang Zhong, Weihong Xing, and Bingbing Zhang. Fabrication of ceramic membranes with controllable surface roughness and their applications in oil/water separation. *Ceramics International*, 39(4):4355–4361, 2013.

Peter L Zock and Martijn B Katan. Hydrogenation alternatives: effects of trans fatty acids and stearic acid versus linoleic acid on serum lipids and lipoproteins in humans. *Journal of Lipid Research*, 33(3):399–410, 1992.

Linda Zou, I Vidalis, D Steele, A Michelmore, SP Low, and JQJC Verberk. Surface hydrophilic modification of ro membranes by plasma polymerization for low organic fouling. *Journal of Membrane Science*, 369(1-2):420–428, 2011.

COLOPHON

This document was typeset using LaTeX. The document layout was generated using the arsclassica package by Lorenzo Pantieri, which is an adaption of the original classicthesis package from André Miede.